AD NUMBER

AD-101 309

CLASSIFICATION CHANGES

TO **UNCLASSIFIED**

FROM **CONFIDENTIAL**

AUTHORITY

OCA; AUG 29, 1974

19990303103

AD NUMBER

AD-101 309

NEW LIMITATION CHANGE

TO **DISTRIBUTION STATEMENT - A**

Approved for public release;
distribution is unlimited.

LIMITATION CODE: 1

FROM **NO CHANGE TO PREVIOUSLY ASSIGNED DISTR ST'MT**

AUTHORITY

USNOL; AUG 29, 1974

[redacted]L
NAVORD Report 3813

Aeroballistic Research Report 253

WIND-TUNNEL MAGNUS CHARACTERISTICS OF THE 7-CALIBER ARMY-NAVY SPINNER ROCKET

Prepared by:

W. Luchuk
W. Sparks

ABSTRACT: A wind-tunnel test program on the 7-caliber Army-Navy Spinner Rocket has been completed in the NOL 40 x 40 cm Aeroballistics Tunnel No. 1. Magnus force and moment measurements have been made at Mach numbers of 0.291, 0.600, 0.810, 0.914, 1.57, 1.77, 1.90, 2.21, and 2.46 and at angles of attack up to 20 degrees. The Magnus measurement problem for the wind tunnel is examined, and a discussion of the instrumentation used to overcome this problem is presented. The results of the test program are presented in coefficient form and a comparison with the results from the Aberdeen Ballistics Ranges is presented. It is shown that there is agreement between the Naval Ordnance Laboratory wind tunnel and the Aberdeen range results at supersonic speeds, and that the Magnus coefficients are non-linear with angle of attack.

U. S. NAVAL ORDNANCE LABORATORY
WHITE OAK, MARYLAND

[redacted]

[redacted]

CE: THIS DOCUMENT CONTAINS INFORMATION AFFECTING THE
ONAL DEFENSE OF THE UNITED STATES WITHIN THE MEANING
HE ESPIONAGE LAWS, TITLE 18, U.S.C., SECTIONS 793 and 794.
TRANSMISSION OR THE REVELATION OF ITS CONTENTS IN
MANNER TO AN UNAUTHORIZED PERSON IS PROHIBITED BY LAW.

[redacted]

[redacted]

NOTICE: THIS DOCUMENT CONTAINS INFORMATION AFFECT
NATIONAL DEFENSE OF THE UNITED STATES WITHIN THE M
OF THE ESPIONAGE LAWS, TITLE 18, U.S.C., SECTIONS 793 ar
THE TRANSMISSION OR THE REVELATION OF ITS CONTENTS
ANY MANNER TO AN UNAUTHORIZED PERSON IS PROHIBITED

NAVORD REPORT

WIND-TUNNEL MAGNUS CHARACTERISTICS OF A CALIBER [illegible]

SPINNER ROCKET

10 SEPTEMBER 19[illegible]

U. S. NAVAL ORDNANCE LABORATORY

WHITE OAK, MARYLAND

This test program was performed at the request of the Bureau of Ordnance (Re3d) and was performed under Task Number NOL-B3d-453-1-55)

This report is a presentation of the Magnus force and moment characteristics of the 7-Caliber AN Spinner Rocket as determined from wind-tunnel measurements.

JOHN T. HAYWARD
Captain, USN
Commander

H. H. KURZWEG, Chief
Aeroballistic Research Department

Contents

Illustrations

[redacted]

Contents (continued)

WIND-TUNNEL MAGNUS CHARACTERISTICS OF THE 7-CALIBER ARMY-NAVY SPINNER ROCKET

INTRODUCTION

1. The 7-caliber Army-Navy Spinner Rocket (Figure 1) is the intermediate length member of a group of three low-drag rocket shapes, whose aerodynamic characteristics are the subject of a joint Army-Navy research program. Measurements, at small angles of attack, of these characteristics have been made in the ranges at the Ballistic Research Laboratories, Aberdeen Proving Ground, at supersonic speeds (references a and c) and at transonic speeds (reference d). The aerodynamic characteristics of the three members of this program have also been measured in a wind tunnel at low subsonic speeds (references b and e). Late in 1952, at the request of the Bureau of Ordnance (Re3d), the Naval Ordnance Laboratory undertook the problem of determining the Magnus characteristics of spinning projectiles. A logical choice of model, on which to perform the first wind-tunnel measurements was the 7-caliber Army-Navy Spinner, since it was a simple shape of typical missile proportions and since there were considerable range data available with which the wind-tunnel data could be compared. The initiation of a program of Magnus measurement necessitated the development of suitable instrumentation not only for the force measurement system, but also for the model rotational power. The problem was accentuated by the smallness of the Magnus force compared to the other forces acting on the model. A discussion of the instrumentation problems and the solutions thereof will be found in the section on instrumentation.

2. These tests were performed in the NOL 40 x 40 cm Aeroballistics Tunnel No. 1 (reference f), an open-jet, intermittent type tunnel. This tunnel was primarily designed for supersonic testing but it can be operated at subsonic speeds by inserting a converging nozzle and using an adjustable diffuser as a throttling valve. Magnus force and moment measurements were made using an "external" strain-gage balance, with an air "coaster"turbine providing the rotational power.

Symbols

C_Y = wind-tunnel side force coefficient = Y/qS

C_ψ = wind-tunnel yawing moment coefficient = Ψ/qSd

C_{M_p} = Magnus force coefficient (at a given angle of attack) = $C_{M_{p\alpha}}\,\alpha$

(Note: All moments are referred to c.g.; see Figure 1)

Symbols (continued)

$C_{N_{p_\beta}}$ = aeroballistic Magnus force coefficient = $\left[(M_{p_\beta})p_\beta\right] / i\left(\frac{pd}{2V}\right) q_\beta S$

C_{M_p} = Magnus moment coefficient (at a given angle of attack) = $C_{M_{p\alpha}} \cdot \alpha$

$C_{M_{p\alpha}}$ = aeroballistic Magnus moment coefficient = $\left[(M_{p_\beta})p_\beta\right] / \left(\frac{pd}{2V}\right) q_\beta Sd$

d = body diameter (0.167 foot)

F = range Magnus force (pounds)

i = vector operator = $\sqrt{-1}$

K_F = range Magnus force coefficient = $F/i\rho u \omega d^3 \beta$

K_T = range Magnus moment coefficient = $-T/\rho u \omega d^4 \beta$

l = model length (1.167 feet or 7 calibers)

M = Mach number

$\left[(M_{p_\beta})p_\beta\right]$ = aeroballistic Magnus moment or yawing moment due to spin velocity at an angle of attack (foot-pounds)

$\left[(M_{p_\beta})p_\beta\right]$ = aeroballistic Magnus force or side force due to spin velocity at an angle of attack (pounds)

p = rotational velocity (radians/second) or (revolutions/second, rps)

q = dynamic pressure = $\frac{\rho V^2}{2}$ (pounds/feet^2)

Re = Reynolds number based on model length = $\frac{Vl\rho}{\mu}$

S = reference body cross-sectional area = $\pi d^2/4$ (feet^2)

T = range Magnus moment (foot-pounds)

u = free-stream velocity-range (feet/second)

V = free-stream velocity = u (feet/second)

Y = wind-tunnel side force (pounds)

α = angle of attack (degrees or radians)

β = angle of yaw (degrees or radians)

Symbols (continued)

ϵ = error notation

$\hat{\beta}$ = aeroballistic and range complex yaw angle = $(\beta + i\alpha)$ (radians or degrees)

γ = free-stream viscosity computed by Sutherland's formula (pound second/feet^2) ($\beta = 0^\circ$ for wind tunnel)

ρ = free-stream air density (slugs/feet^3 = #sec^2/feet^4)

ω = range rotational velocity = p (radians/second)

ψ = wind-tunnel side or yawing moment (foot/pounds)

INSTRUMENTATION

3. Only the more important features of the instrumentation are given in this discussion and none of the preliminary tests which led to the design of the present instrumentation are described. However, the instrumentation described below was preceded by several preliminary set-ups, each of which yielded information that indicated the need for changes or additions to the equipment, and although the present set-up will yield data of sufficient accuracy and reliability for some purposes, the set-up is not an "ideal" solution (see uncertainty estimate, paragraph 30) for the measurement of Magnus effects on spinning models. Further development is required and is now being carried out. In the future, data of more reliability and accuracy should be obtained because of improved instrumentation, test techniques, and more varied test conditions such as testing at plus and minus angles of attack, testing with plus and minus spin directions, etc.

4. A sketch of the model, balance, and support system is presented in Figure 2. The instrumentation used inside the wind tunnel in this test is divided, for the purpose of this discussion, into the following parts:

(a) A sting-supported spinning model, mounted on ball bearings and powered by an air turbine wheel in the base of the model (see Figure 3).

(b) A strain-gaged sting with the gage sections located immediately behind the model (see Figure 4).

(c) A tachometer pickup which has an A.C. voltage output of the same frequency as the model rotation (see Figure 3).

(d) A support system which permitted a small variation of the angle of yaw as well as variation in the angle of attack,. The variation in yaw angle removed any trim angle in the yaw plane (see Figure 5).

5. The model used in this test consisted of a thin aluminum shell mounted on two high-speed ball bearings. A magnetized steel ring

was mounted inside the model and rotated with the model to induce an alternating e.m.f. in the stationary tachometer pick-up coil. An air turbine rotor attached to the model near the base provided the model rotational power. Maximum spin rates of about 36,000 rpm were used in these tests; higher spin rates can be obtained, if desired, with motive power of this type. The other components located inside the model were non-spinning and consisted of a sting extension on which the bearings, the tachometer pick-up coil, and the turbine air-inlet nozzle unit were mounted. The high pressure turbine air (over 100 psi) was supplied to the model through the hollow sting. After passing through the turbine blades, the air was exhausted through the base of the model. The following are among the more important requirements which were met as far as possible in the design and manufacture of the model and model components:

(a) the spinning model shell was made as light as possible and the concentricity of all surfaces was held to a close tolerance to minimize any mass unbalance which might induce vibrations;

(b) the support bearings were widely separated to reduce "run-out" in the model due to "slop" in the bearings and thus minimize dynamic unbalance due to run-out;

(c) the spinning tachometer magnet was made of hardened steel since it was learned that Alnico magnets would explode at the spin rates attainable with air turbine drives;

(d) the model-motor combination was capable of being dynamically balanced by the addition of small weights in two transverse planes, one of which was located near the nose and the other was located near the rear of the model. At each of these transverse planes, there was a ring of tapped holes into which small set screws could be inserted to effect the dynamical balance. These holes were, of course, inside the model.

6. The sting used in this test contained two strain-gaged yaw sections (see Figure 4). The strain-gage bridge for the front section gave a D.C. signal voltage proportional to the yawing moment about a point 0.68 calibers in front of the base of the model. The aft strain-gage bridge gave a D.C. signal voltage proportional to the yawing moment about a point 3.80 calibers behind the base of the model. To eliminate any possible effects of air loads on the balance itself, it was enclosed in a windshield which extended forward from the sector into the base of the model (see Figure 4). The long, hollow sting was made in several sections which were assembled and silver soldered together before the strain gages were mounted. This type of construction was necessary in order to provide a sufficiently large air passage through the sting and to permit the machining of gage-section walls of thicknesses sufficient to insure relatively high sensitivity to applied yaw loads and yet provide adequate strength for high pitch loads.

7. The tachometer pick-up coil consisted simply of a small coil of fine wire wound around a soft iron core. One end of the core was mounted with only a few thousandths of an inch clearance between it and the spinning magnet so that with the model (and magnet) spinning, an alternating e.m.f. was induced in the pick-up coil (see Figure 3).

8. The sting-mounted model was clamped in a so-called zero-yaw device which permitted a $\pm$ 2 degrees adjustment in the yaw angle (see Figure 5). This device was in turn clamped to the sector with which the angle of attack is varied. When the model is installed in the tunnel there may be, and in fact usually is, a small angle in the yaw plane between the model axis and the air flow. This angle, usually one half degree or less, can be tolerated for most wind-tunnel tests since its effects can be removed from the final data. However, with a sensitive balance such as is required for Magnus measurements the moment due to this yaw angle may be large compared to the Magnus moment and may introduce difficulties in accurately recording the data. Therefore, the zero-yaw device is used in Magnus measurements to eliminate moments in the yaw plane.

9. The instrumentation used outside the tunnel in this test is divided, for the purpose of this discussion, into the following parts: (see Figure 6).

(a) A pre-amplifier to amplify the voltage of the tachometer signal.

(b) An audio frequency oscillator to provide calibration frequencies for use with the tachometer instrumentation.

(c) An events-per-unit-time counter to measure either the calibration frequencies or the amplified tachometer output frequency.

(d) An oscilloscope to monitor the amplified tachometer signal.

(e) An electronic tachometer to convert the amplified alternating voltage from the pick-up coil into a direct current voltage proportional to the model spin frequency.

(f) A servo system to position the recorder chart as a function of the model spin rate and in so doing, null out the D.C. voltage of the electronic tachometer.

(g) A 6 volt battery to apply a D.C. voltage across the strain-gage bridges.

(h) A nulling and calibration circuit for each strain-gage bridge.

(i) A D.C. amplifier for each strain-gage bridge to amplify the unbalance voltage between the bridge and nulling circuit; the unbalance is indicative of any moment, due to air loads, about that strain-gage section.

(j) A two channel recorder which had been modified as stated in paragraph 19 below, to make the chart position a function of a third variable.

10. Any high gain amplifier is adequate for amplifying the pick-up coil signal. In this test a General Radio Amplifier was used. For future tests the use of a Techtronic direct coupled pre-amplifier is planned since this pre-amplifier has built-in circuits to remove any undesired frequencies (in this case sirty cycle pick-up which gives trouble at low rotational speeds where the tachometer voltage is low and high amplification is required).

11. A Hewlit Packard Audio Frequency Oscillator was used to provide calibration frequencies. In obtaining Magnus data the oscillator was used in the following manner; for zero frequency, the chart was set to a zero position. The oscillator was set to the desired top frequency to be used in the test, in this case 600 cycles per second, and then switched into the tachometer circuit. The chart servo system would position the chart at the point corresponding to 600 cycles per second. The distance between the zero frequency chart position and the 600 cycle per second chart position provided the scale factor for chart position versus spin rate. The oscillator was also set at 500, 400, 300, 200, and 100 cycles per second to check the linearity of chart position with spin rate. It was found that the chart position uncertainty was approximately $\pm$ 1 per cent.

12. An events-per-unit-time counter, called an EPUT Meter, was used as a standard frequency or spin-rate measuring device. This instrument, produced by the Berkely Instrument Company, is accurate to the nearest count. In this test it was set to count cycles per second and was used to check output frequency of the audio oscillator and the model spin rate.

13. A Dumont Oscilloscope was used to monitor the amplified tachometer signal. This instrument had two purposes: (a) it could be used as a voltmeter by comparing the peak voltage of the amplified signal with a calibrating voltage available in the oscilloscope, (an A.C. voltage of at least 5 volts is required for correct operation of the electronic tachometer), and (b) it was used to detect the presence of harmonics in the amplified pick-up coil signal (the General Radio Electronic Tachometer will count harmonics as well as fundamental frequency and thus give an erroneous frequency reading if the amplitude of the harmonics is excessive).

14. The amplified pick-up coil output was fed into a General Radio Electronic Tachometer. This instrument has an indicating meter (a D.C. milliammeter) which indicated the frequency of the A.C. signal connected to its input. Instead of reading the deflection of the indicating meter, the voltage drop across the meter was used to provide a D.C. voltage, proportional to the model spin rate, which could be used as a signal to operate the recorder chart, positioning servo system.

15. A servo system which positioned the recorder chart as a function of the model spin rate was the final part in the tachometer system. This servo system was built around a Leeds and Northrup

Speed-o-max Amplifier and a pen-drive motor. The signal obtained from the General Radio Electronic Tachometer was nulled against the voltage drop across a helipot. The helipot was geared to the recorder-chart drive system. Therefore, when a steady model spin rate was attained the servo system would drive the chart to a fixed position and rotate the helipot to the position required to null out the signal obtained from the electronic tachometer. Since the helipot was geared to the chart drive, this means that the chart position was a function of the model-spin rate. However, if the model-spin rate was continuously increasing or decreasing as in this test, the servo system would never attain this null condition but would always be slightly "behind" the true null position. This introduced a "hysteresis" effect between increasing and decreasing spin directions. By regulating the gain of the servo amplifier and the voltage across the nulling helipot it was possible to decrease the width of the "hysteresis" loop to approximately the width of the recorder pen line for the rotational accelerations used. This slight error introduced no significant uncertainty into the data. Controls were provided to adjust both the chart zero position, and chart spin-rate scale factor (see Figure 7).

16. The strain-gage bridges were powered by a 6 volt battery. No provision was made for regulating this voltage, and therefore, the voltage must have decreased continuously with time. To take this into account, the chart calibration curve for strain-gage bridge unbalance was repeated at frequent intervals during the test. It was found, however, that the chart calibrations did not change with time (within the accuracy of the calibration) even over 5 days of continuous testing, which indicated that the decrease in battery voltage was insignificant. D.C. power to the strain-gage bridges was used for several reasons. Preliminary tests indicated that zero shifts in the electrical balance of the bridges due to temperature effects, were of the same order of magnitude for either A.C. or D.C. power. With D.C. power to the gages, D.C. amplifiers with highly filtered input circuits could be used. With an A.C. system, the amplified bridge signals showed large variations near all resonant-vibrational frequencies of the model and sting as well as large variations at all multiples and sub-multiples of the strain-gage carrier frequency.

17. A nulling and calibration circuit was provided to "zero out" any initial unbalance in the bridge circuits and provide a means of calibrating the balance that is independent of applied voltage to the bridge.

18. A Leeds and Northrup D.C. Amplifier was used for each strain-gage circuit. These amplifiers are equipped with input circuits which filter out any A.C. components in the strain-gage signals. This eliminated the troubles mentioned above in paragraph 16. It was also found that the use of these D.C. amplifiers permitted higher amplification factors because of their greater stability and because of their greatly simplified nulling and calibration circuits as compared to the phase shifting circuits required with A.C. strain-gage power. These D.C.

amplifiers contained built-in step switches, the use of which made available a range of amplification factors each of which has a known and exact multiple of the others. This feature simplified data taking in that the amplification could be changed over a wide range of values without recalibration.

19. A two-channel Leeds and Northrup Speed-o-max Recorder was used to record the data. This recorder as purchased from the manufacturer was equipped with both a time-drive system and a selsyn-drive system for the chart. That is, the chart position could be a function of time with chart speeds of either one inch per minute or thirty inches per minute, or the chart could be positioned with the selsyn motor. This latter method of positioning the chart essentially converted the recorder to an X_1, X_2, and Y recorder, that is, two variables could be directly recorded as functions of a third variable, provided that the third variable could be related to the rotational angle of the selsyn generator controlling the position of the selsyn motor in the chart drive system. The two pen recorder converted to an X_1, X_2, Y recorder, is particularly suitable for recording data such as Magnus forces continuously as functions of model angle of attack. However, this selsyn system is not easily adaptable to recording an independent or "Y" variable which is available as a D.C. voltage. Therefore, a servo system was made to position the chart with a D.C. voltage. The chart-drive selsyn motor was replaced with a servo motor and with this change the recorder could then plot two variables each as a function of a third, each dependent variable (X_1 or X_2) being a D.C. voltage between 0 and 10 millivolts.

Test Technique

20. The model used in these tests had an air "coaster" turbine for its rotational power. The term "coaster" means that this model was designed to be brought up to a certain speed before the wind-tunnel blow was started. Then with the angle of attack set at some nominal value, the blow was started and flow established, the high pressure supply air to the turbine was cut off and the model's rotational speed allowed to "decay" during the duration of the blow. Strain-gage balance data were continuously recorded as functions of spin. This type of data-taking procedure was intended to avoid any possible effect of turbine power on the strain-gage balance. The disadvantage of this procedure was that the speed decrement during "coast-down" was small, thus requiring several wind-tunnel blows to cover the desired rotational speed range, for each angle of attack. This model-motor-balance combination was checked for turbine-power effects on the balance by running up the rotational speed with the wind off and noting the balance output. The rotational speed had no effect on the strain-gage balance. With this fact established a "power on" type wind-tunnel blow was attempted. This "power on" type blow revealed: (a) that the "power on" rotational acceleration was much greater than the deceleration which occurred during a "coast down" type blow, (b) that a higher maximum rotational speed could be attained. These "power on" effects were probably a result of the increase in maximum power that the turbine

could develop, due to the reduced back pressure to the air turbine caused by reduced ambient air pressure in the wind tunnel during the blow. This increase in turbine power made it possible to cover a larger speed range in a single blow, thereby cutting down the required wind-tunnel time by a considerable amount. These conditions were sufficient to warrant the performance of this type of blow for the entire program. At one test condition $M = 0.291$, $\alpha = -21$ degrees, a completely non-linear set of recorder traces were obtained, which looked unusual. This condition was repeated and test data were taken for two "power up" type blows and a single "coast down" type blow. The data are presented in Figure 9 as further justification of the "power up" type blow.

21. This test program did not include Mach numbers higher than 2.46 because: (a) the maximum Magnus force that this size model was able to develop was approaching zero, and (b) the balance used did not have the extreme sensitivity required to measure these minute forces. Four subsonic Mach numbers were chosen to cover the entire subsonic range with special emphasis on the high subsonic end, where aerodynamic characteristics usually have the largest variations. The angle of attack range for this program was approximately +4 degrees to -21 degrees. This sign designation was used strictly for convenience in the wind tunnel.

Coefficients

22. The definitions for side force and yawing moment coefficients (in this case due to Magnus, i.e., due to spin at an angle of attack) in use in the Naval Ordnance Laboratory wind tunnels are

$$C_Y = \frac{Y}{qS} \qquad \text{Side force coefficient}$$

$$C_{Y'} = \frac{Y'}{qSd} \qquad \text{Yawing moment coefficient}$$

23. The aeroballistic Magnus force and moment coefficients as defined in references (g) and (h) are

$$C_{N_{p\alpha}} = \frac{\left[N_{p\phi} \cdot p\dot{\phi}\right]}{i\,\dot{\phi}\left(\frac{pd}{2V}\right) qS} \qquad \text{Magnus force coefficient}$$

$$C_{M_{p\alpha}} = \frac{\left[M_{p\phi} \cdot p\dot{\phi}\right]}{\dot{\phi}\left(\frac{pd}{2V}\right) qSd} \qquad \text{Magnus moment coefficient}$$

24. The ballistic Magnus force and moment coefficient definitions as given by references (g) and (h) (see also reference (i)) are

$$K_F = \frac{F}{i\,\phi\,\rho\,u\omega d^3} \qquad \text{Magnus force coefficient}$$

$$K_T = \frac{-T}{\phi\,\rho\,u\omega d^4} \qquad \text{Magnus moment coefficient}$$

25. From these definitions, for the same angle of attack (or yaw) with respect to the wind vector, the following relations, valid for the wind-tunnel case, can be arrived at

$$C_{M_{Pa}}\alpha = -\left[C_Y\right]\left(\frac{2V}{pd}\right) = K_F \alpha \frac{16}{\pi}$$

$$C_{M_{Pa}}\alpha = +\left[C_Y\right]\left(\frac{2V}{pd}\right) = -\left[K_T\right]\alpha \frac{16}{\pi}$$

{in the case of the wind tunnel $\beta = 0$ i.e., $\phi = \alpha$}

The brackets in the above relations are included to indicate that these quantities may have either a positive or negative sign, and that the sign which precedes them is there as part of the definition.

26. If the simple two dimensional picture of the Magnus effect is considered to be acting on a spinning body at an angle of attack, the above coefficients will have the following signs.

Center of Magnus Ahead of Center of Gravity

	+p, +α	-p, -α	+p, -α	-p, +α
C_Y	-	-	+	+
$C_{M_{Pa}}$	+	+	+	+
K_F	+	+	+	+
C_Y	-	-	+	+
$C_{M_{Pa}}$	-	-	-	-
K_T	+	+	+	+

Center of Magnus Behind the Center of Gravity

	+p, +α	-p, -α	+p, -α	-p, +α
C_Y	-	-	+	+
$C_{M_{P\alpha}}$	+	+	+	+
K_P	+	+	+	+
$C_{Y'}$	+	+	-	-
$C_{M_{P\alpha}}$	+	+	+	+
K_T	-	-	-	-

Data Reduction

27. The raw data, taken at fixed values of angle of attack, were "linear" with rotational velocity with only a single exception. This greatly simplified the data reduction by making it possible to reduce the data by "slopes." Instead of taking particular points on the recorder traces, straight lines were faired over the traces and these slopes converted to coefficient slopes. These coefficient slopes were the change in side force coefficient and yawing moment coefficient, C_Y and $C_{Y'}$, respectively, with spin (i.e., dC_Y/dp $dC_{Y'}/dp$). From these, the Magnus coefficients were obtained

$$C_{M_{P\alpha}} \cdot \alpha = - \left[\frac{dC_Y}{dp}\right]\left(\frac{2V}{d}\right) = C_{M_p}$$

$$C_{M_{P\alpha}} \cdot \alpha = + \left[\frac{dC_{Y'}}{dp}\right]\left(\frac{2V}{d}\right) = C_{M_p}$$

It is to be noted that the above coefficients, C_Y, $C_{Y'}$, C_{M_p}, C_{M_p}, $C_{M_{P\alpha}}$, and $C_{M_{P\alpha}}$ are all non dimensional.

28. The only correction applied to the data was the shifting of the curves to the trimmed angle of attack condition. A correction to the indicated angle of attack due to pitch plane loads was determined and found to be only 0.3 degrees at an indicated angle of attack of 22 degrees, at M = 1.56, the condition of greatest pitch loads. This correction to the indicated angle of attack amounted to less than

2 percent at most, and would not contribute significantly to the improvement of the data. It was, therefore, omitted. It should also be noted that this correction was computed using no-spin static pitch force and moment data taken during another program. Corrections to the data due to pitch or yaw interactions were not required with the strain-gage balance used, since these interactions were removed by electrical shunting in the balance bridge circuits (see reference j).

29. The standard right-hand coordinate system, as used by the National Advisory Committee for Aeronautics and the Ballistic Research Laboratories, was adopted to define the orientation of the model in the wind tunnel and establish the sign conventions. This system is shown in Figure 8 (see references g and h).

Accuracy

30. No computation has been made to determine absolute probable errors for these data, however an indication of the accuracy based on the repeatability has been made. The coefficients C_{N_p} and C_{M_p} were taken in two groups; one group of data being that which was included in the angle of attack range from +4 degrees to -8 degrees; and the other group of data being, that which was obtained at angles of attack from α = -8 degrees to α = -21 degrees. This grouping was done for all Mach numbers. On this basis the average deviations in the coefficients C_{N_p} & C_{M_p} were:

	C_{N_p}	C_{M_p}
$-8^\circ \leq \alpha \leq +4^\circ$	± 0.0085	± 0.0138
$-21^\circ \leq \alpha < -8^\circ$	± 0.0181	± 0.0316

If these deviations were considered as average deviations in percent of the measured coefficients the result would be

	$\epsilon_{C_{N_p}/C_{N_p}}$	$\epsilon_{C_{M_p}/C_{M_p}}$
$-8^\circ \leq \alpha \leq +4^\circ$	± 9.2 percent	± 35.0 percent
$-21^\circ \leq \alpha < -8^\circ$	± 2.3 percent	± 6.3 percent

That the percent error should be larger for the low angle of attack range is to be expected, since the coefficients are approaching zero. A better estimate of the accuracy of measurement might have been obtained if the percent deviations were determined using the actual forces and moments, and considering the data as being part of a large force and moment group and a small force and moment group. This would have been a more realistic estimate in view of the fact that at high subsonic speeds and relatively low angles of attack appreciably larger forces and moments were

obtained than at high Mach numbers and high angles of attack. Unfortunately, due to the lack of a sufficient number of repeat points at all angles and at all Mach numbers, an adequate statistical error analysis was not practicable.

Results

31. A complete definition of the wind-tunnel test conditions is presented in Table I in which the Reynolds number (based on the model length of 14 inches), the dynamic pressure, the flux density on mass flow per unit area (ρV), and the maximum Magnus force and moment measured at 600 revolutions per second, are tabulated for each Mach number.

32. The "basic" side force and yawing moment coefficients, (about the center of gravity) C_Y and C_{ψ}, are presented in Figures 10 to 19 as functions of the rotational velocity, p (revolutions per second), for constant angles of attack. This is in the same general form as the raw data were obtained during the actual testing. The alternate plots of C_Y and C_{ψ} are arranged in the order of increasing Mach number from M = 0.291 to M = 1.56. These figures reveal that the Magnus characteristics of this configuration exhibited an orderly behavior with spin rate, angle of attack, and Mach number; the figures also show certain noteworthy features of both the subsonic Magnus characteristics and the supersonic Magnus characteristics, which will be discussed below.

33. Generally speaking, the data obtained at M = 0.291 (Figures 10 and 11) exhibit the most marked variations in Magnus characteristics for all the Mach numbers tested. It can be seen from these two figures that at small angles of attack, the Magnus characteristics are linear with spin rate. As the angle of attack is increased, the linearity of the Magnus characteristics with spin persists but only up to a certain spin velocity. At this point the data abruptly take on a different linear relationship with spin. This "bi-linear" behavior continues with increase in angle of attack until at an angle of attack of -21 degrees the Magnus variation with spin becomes completely non-linear. The next pair of Figures, 12 and 13, present the basic coefficients at M = 0.600. These curves are essentially the same as those for M = 0.291 except that the non-linear behavior at α = -21 degrees has become "bi-linear." The magnitudes of the coefficients in these plots are slightly larger than those presented at M = 0.291. Figures 14 through 17 present the data obtained at M = 0.810 and 0.914. The general form of these curves is the same as the curves for M = 0.600 except that the magnitudes of the coefficients have grown larger with the increasing Mach number. One general effect which can be observed is that the "break" in the curves becomes less pronounced with increasing Mach numbers. The occurrence of the "break" or "corner" in the subsonic data is at present unexplainable. The points at which these "breaks" occur are not accurately defined because of fluctuations in the recorder traces due to model vibration and tunnel turbulence, and because the change in the actual recorder trace slopes for most cases is small.

34. The plots of C_Y and C_{Y_p} at M = 1.57, Figures 18 and 19, are included to show the marked linearity of these coefficients with spin, even at the highest angles of attack, as contrasted to the "bi-linear" variations at subsonic speeds. The primary coefficients for the higher supersonic Mach numbers are identical in form to those presented in Figures 18 and 19. They are not presented here since it is felt that the data at M = 1.57 are sufficiently representative of all the supersonic Mach numbers.

35. The next group of figures present the Magnus force coefficients, C_{N_p}, the Magnus moment coefficients, C_{M_p}, and the center of Magnus. These coefficients may be written as

$$C_{N_p} = C_{N_{p_\alpha}} \cdot \alpha = -C_Y \left(\frac{2V}{pd}\right) \qquad C_{M_p} = C_{M_{p_\alpha}} \cdot \alpha = C_{Y_p} \left(\frac{2V}{pd}\right)$$

These coefficients are the next logical step in the data reduction since they are essentially the slopes of the basic coefficients. The subsonic Magnus coefficients are presented in Figures 20 to 23; solid curves have been faired through the points which represent the initial slopes, up to the break, of the basic coefficient curves. Dashed curves have been faired through those points which represent the slopes ("secondary" slopes) of the basic coefficient curves after the "breaks." The "secondary" slope points for M = 0.291 have not been included in Figure 20 because their erratic behavior defines no distinct curve. This group of subsonic figures reveals that there is a smooth variation of C_{N_p} and C_{M_p} with angle of attack (even for the "secondary" slopes) and a gradual increase in the magnitude of the coefficients with increasing Mach number. The increase in coefficients with Mach number has already been pointed out in the previous discussion of the subsonic basic coefficients. C_{N_p} and C_{M_p} at M = 0.291, M = 0.600, and M = 0.810 appear to be increasing with angle of attack and give no hint of a peak or maximum within the angle of attack range tested, but at M = 0.914 at the highest angles there seems to be a suggestion of a peak in the C_{N_p} curve. It would be interesting in the future to make measurements at higher angles of attack to determine, if and where, the Magnus coefficients attain a maximum value. The supersonic plots of C_{N_p} and C_{M_p} are presented in Figures 24 to 28. These curves have the noteworthy difference from the subsonic curves in that at angles of attack between 10 degrees and 14 degrees the Magnus coefficients have attained their greatest value. Further increase in angle of attack is accompanied by a diminution of the coefficients. Although there are relatively few Magnus data at the positive angles of attack, the C_{N_p} and C_{M_p} variations appear to be odd functions of the angle of attack, i.e., the curves have origin symmetry. It seems that at small angles of attack the data might be fitted by a polynomial in α of the form $A\alpha + B\alpha^3$.

36. Also presented with the Magnus coefficients in this group of figures, are the variations in center of Magnus with angle of attack; the center of Magnus positions are given in terms of fractions of body length from the base. The curves of the subsonic centers of pressure show a small rearward movement at the higher angles of attack and practically

no variation with Mach number. The curves of the supersonic centers of Magnus have a small "s" variation with angle of attack and also no significant change with Mach number. There is only approximately a 10 percent of the model length (or .7 calibers) variation in the center of Magnus for all Mach numbers tested, if the data points at the small angles of attack, whose scatter would normally be expected to be large, are not included. The center-of-Magnus curves have been faired to that value of center of Magnus as determined by the Magnus force and moment coefficient slopes at $\alpha = 0^{o}$.

37. The next group of Figures (29 to 37), present the Magnus force and moment coefficients in the form $C_{N_{p\alpha}}$ and $C_{M_{p\alpha}}$. These curves were constructed using the faired curves of C_{N_p} and C_{M_p} and using the relationships, $C_{N_{p\alpha}} = \frac{C_{N_p}}{\alpha}$ and $C_{M_{p\alpha}} = \frac{C_{M_p}}{\alpha}$. These relationships yield "secant-slope" values of $C_{N_{p\alpha}}$ and $C_{M_{p\alpha}}$ at all angles of attack other than zero degrees. At $\alpha = 0$ degrees, these "secant-slope" coefficients are the actual slopes of the C_{N_p} and C_{M_p} curves, i.e., $\left(C_{N_{p\alpha}}\right)_{\alpha=0^{o}} = \left(\frac{dC_{N_p}}{d\alpha}\right)_{\alpha=0^{o}}$ and $\left(C_{M_{p\alpha}}\right)_{\alpha=0^{o}} = \left(\frac{dC_{M_p}}{d\alpha}\right)_{\alpha=0^{o}}$. For the secondary slopes (as previously discussed) the above relationships were also used. These curves behave like even functions of the angle of attack and have the appearance of parabolas at the small angles. The Magnus force coefficient $C_{N_{p\alpha}}$ as defined in the table presented in the section titled "Coefficients" is positive in sign regardless of the sign of the angle of attack or the sign of the spin velocity. The Magnus moment coefficient $C_{M_{p\alpha}}$ is similarly independent of the signs of angle of attack and spin velocity (or combinations thereof) and depends only on the location of the center of Magnus with respect to the center of gravity. $C_{M_{p\alpha}}$ is positive if the center of Magnus is located behind the center of gravity and negative in sign if the center of Magnus is ahead of the center of gravity.

38. Included in these plots are the values of $C_{N_{p\alpha}}$ and $C_{M_{p\alpha}}$ as obtained from free-flight range firings (reference c).* The range values are shown in these figures as horizontal lines between $\alpha = \pm 3$ degrees because these data were obtained from range-firing rounds whose angular oscillations varied approximately between these limits.

39. An overall picture of the test results can be obtained from Figures 38 and 39. In these figures C_{N_p} and C_{M_p} are plotted against Mach number for various angles of attack. The subsonic portions of these plots present curves for angles of attack up to 20 degrees, while the high angle of attack curves have been omitted from the supersonic portion. This was done to preserve the clarity of the presented supersonic curves since the higher angle-of-attack curves would be superimposed over the presented curves and would be confused with them.

* BRL 876 contains only supersonic data

40. During the processing of the data it was noticed that the peak supersonic values of C_{N_p} plotted against Mach number could be approximated by $1/\sqrt{M^2-1}$. This relation was included in Figure 38 to demonstrate this approximation. The authors do not wish to imply that this relationship would hold for all models, but it does appear that

$$(C_{N_p})_{max} = K/\sqrt{M^2-1}$$

might be a relationship which would describe the maximum Magnus coefficient obtainable at supersonic velocities, where K might be a function of the model shape and fineness ratio ($K \approx 1$ for this model). Further evidence should be sought to check the validity of this apparent relationship.

41. In Figure 40 are presented $C_{N_{P\alpha}}$ and $C_{M_{P\alpha}}$ values versus Mach number for small angles of attack from the Naval Ordnance Laboratory wind tunnel and the Ballistic Research Laboratories firing range results.

42. Before giving some comments on the comparison between the results presented in this report and the Aberdeen ballistic range determination of the Magnus characteristics of the seven caliber AN Spinner Rocket, some clarification may be in order for Figure 40. In this figure the data points with the square symbols are the values of $C_{N_{P\alpha}}$ and $C_{M_{P\alpha}}$ derived from the wind-tunnel C_{N_p} and C_{M_p}-coefficient values for α equal to 4 degrees. The curves fitted to these points are curves fitted by eye to the points and are only presented to illustrate the general trend of the data with Mach number. The data points with circle symbols are the values of $C_{N_{P\alpha}}$ and $C_{M_{P\alpha}}$ coefficients derived from the wind-tunnel C_{N_p} and C_{M_p}-coefficients versus α slopes at α equal to 0 degrees. Again, the curves through these points have been fitted by eye and illustrate the general trend of the wind-tunnel data with Mach number. The shaded triangles represent data points taken from BRL Report 876, pages 53-70, and converted to $C_{N_{P\alpha}}$ and $C_{M_{P\alpha}}$ coefficients (see section on "Coefficients" for the relationships used to convert K_F and K_T to $C_{N_{P\alpha}}$ and $C_{M_{P\alpha}}$ coefficients). The Ballistic Research Laboratories curves fitted to these points were fitted by a statistical method that was fairly involved and, therefore, is not explained here. The shaded diamonds represent data points taken from BRL Report 775, pages 19-24, and converted to $C_{N_{P\alpha}}$ and $C_{M_{P\alpha}}$ coefficients. The curves fitted to these points were fitted by a statistical method that was also fairly involved and is, therefore, not explained here (see BRL Report 876 and BRL Report 775 for the methods used for fitting curves to these data).

43. Since (a) no analysis has been made of the data presented in this report; (b) there are several obvious differences between the experimental conditions existing for a sting mounted model in the NOL 40 x 40 cm Aeroballistics Tunnel and a model fired in the BRL Ballistics Range; and (c) there are differences in the data reduction procedures

between the wind-tunnel and free-flight data presented in Figure 40, no direct comparison should be expected. However, the correlation between these data shows some trends which appear to be significant and are therefore mentioned below.

44. For the reasons listed in the preceeding paragraph, no detailed comparison of the wind-tunnel and firing-range data is given or warranted; hence, let it suffice for the authors to state the following:

(a) At supersonic Mach numbers, the range and wind-tunnel values for both $C_{M_{p\alpha}}$ and $C_{M_{A\alpha}}$ are essentially in agreement within the experimental accuracy of the data.

(b) The subsonic Magnus force coefficients, as determined by the wind tunnel do not agree with the values determined by the ballistic range in that the wind-tunnel Magnus force coefficients appear to be significantly larger than the Magnus force coefficients determined from range firings.

(c) As regards the subsonic Magnus moment coefficients, the wind-tunnel and firing-range results are in complete disagreement. The difference between these results in Magnus moment signs indicates that the firing-range centers of Magnus are ahead of the projectile center of gravity (C.G. 4.04 calibers from the nose) whereas the wind-tunnel centers of Magnus are behind the projectile center of gravity. Generally speaking, the wind-tunnel results show that there is relatively little change in center-of-Magnus position for the Mach numbers for which data were obtained; on the other hand, the firing-range results show a rather large variation, with Mach number, in center-of-Magnus position. The reason for this difference between wind-tunnel and firing-range results is, as present, unknown.

45. Figures 41 and 42 present some typical schlieren photographs taken during the program. All of the photographs were taken as Ektachrome color transparencies using an experimental color schlieren system. The black and white photographs presented here were reproduced from black and white negatives made from the Ektachrome transparencies and are not as good in quality as ordinary black and white schlieren photographs, due to the successive reproductions and to the poorer initial quality of the Ektachrome transparencies. Color schlieren transparencies however, do reveal variations in the flow patterns to a much greater extent than do black and white schlieren photographs due to the ability of the human eye to differentiate changes in color better than gradations of black and grey. Figure 41 presents two subsonic schlieren photographs of the model at $\alpha \approx 21$ degrees and a spin rate of approximately 500 revolutions. One photograph was taken when the Mach number was 0.810 and the other was taken when the Mach number was 0.914. The only marked difference between the two is the increase in the density gradient over the shoulder of the model and the development of the standing shock waves in this vicinity. Figure 42 presents a comparison, at $M \approx 1.57$, of the flow patterns around the model between a high spin case and a no spin case. There is no

apparent difference in the vortex patterns shed from the model between the two, although there is a distinct difference in the flow patterns immediately behind the model base. The difference in the base-wake patterns between the high-spin case and the no-spin case is attributable to the turbine air supply being exhausted out of the model base in the spin case.

CONCLUSIONS

46. The data presented in this report were obtained as an intermediate step in the development of instrumentation for the measurement of Magnus effects on the NOL 40 x 40 cm Aeroballistics Tunnels. The preliminary phases are now complete; i.e., Magnus measurements can now be made with relative ease at typical scaled spin rates and for angles of attack from zero to ninety degrees. Much work remains to be done, however, in improving the accuracy of the data, and in adapting the instrumentation, support system, and motive power to various missile shapes of interest. This further development is now being carried on but the authors believe that the data presented in this report are of sufficient interest for publication at this time.

47. It should be evident from these data that the aeroballistic Magnus coefficient definitions are inadequate for non-linear Magnus data (see references g and h). An analysis of these and similar Magnus data may yield coefficients which remove much of the non-linearities with Mach number, spin rate, and angle of attack.

48. The authors believe that Magnus data obtained from wind-tunnel tests are of at least equal accuracy and reliability to Magnus data obtained from free-flight range firings. However, the direct applicability of these supersonic wind-tunnel Magnus data to the motion of a spinning missile in free flight remains to be demonstrated.[1] Since the Magnus data obtained from wind-tunnel tests essentially agree with free-flight range results for the small angle of attack region; i.e., $\alpha < 3$ degrees, it is reasonable to expect good agreement between free-flight motion predicted from wind-tunnel data and the actual free-flight motion of the missile at such small angles of attack. There is some evidence to believe that a similar conclusion may be forthcoming for free-flight motions involving considerably larger angles of attack than those obtained in firing ranges.[1] Wind-tunnels have an advantage over firing ranges in that not only may wind-tunnel Magnus data be obtained over wide ranges of angles of attack, spin rates, and Mach numbers, but it is also possible

[1] Similar Magnus data from a subsonic wind-tunnel test of the 6" Test Vehicle and the 12.75" Antisubmarine Rocket have recently been obtained by the Naval Ordnance Laboratory. These data are being used at Dahlgren to predict the free-flight motion of the missile by numerical integration of the equations of motion. The computed results have been found to be consistent with observed flight behavior.

since these variables may be treated as completely independent, to exercise a much greater and more careful control over wind-tunnel experimental conditions than may be exercised in the firing ranges. In addition the wind tunnels require no assumptions as to the nature of the variation of aerodynamic forces in order to reduce the data. At the present time such assumptions are made in reducing free-flight range data.

REFERENCES

(a) Turetsky, R. A. "Dynamic Stability of Spinner Rocket Models Fired in the Free-Flight Aerodynamics Range" APG-BRL Memorandum Report No. 526 (Conf) (1950)

(b) Kelly, H. R. and Mercereau, J. R. "The Subsonic Aerodynamic Characteristics of Several Spin-Stabilized Rocket Models II. Magnus Coefficients" NOTS TM 376 (Conf) (1952)

(c) Murphy, C. H. and Schmidt, L. E. "The Effect of Length on the Aerodynamic Characteristics of Bodies of Revolution in Supersonic Flight" BRL Report No. 876 (Conf) (1953)

(d) Schmidt, L. E. and Murphy, C. H. "The Aerodynamic Properties of the 7-Caliber Army-Navy Spinner Rocket in Transonic Flight" BRL Memorandum Report No. 755 (Conf) (1954)

(e) Greene, J. E. "Static Stability and Magnus Characteristics of the 7-Caliber AN Spinner Rocket and the 5" HCSR at Low Subsonic Speeds" NAVORD Report 3884 (Conf) (Unpublished)

(f) Lightfoot, J. H. "The Naval Ordnance Laboratory Aeroballistic Research Facility" (1950) (Restr)

(g) Nicolaides, J. D. "On the Free-Flight Motion of Missiles Having Slight Configurational Assymetries" BRL Report No. 858 (Unclass) (1953)

(h) Nicolaides, J. D. "Correspondence Between the Aerodynamic and Ballistic Nomenclatures" Bureau of Ordnance Note (Unclass) (1954)

(i) McShane, E. J., Kelly, J. L., and Reno, F. V. "Exterior Ballistics" University of Denver Press (1953)

(j) Shantz, I., Gilbert, B. D., and White, C. E. "NOL Internal Strain-Gage Balances Used in the NOL 40 x 40 cm Aeroballistics Tunnels" NAVORD Report 2972 (Unclass) (Unpublished)

TABLE I

Test Conditions and Maximum Force and Moments Measured

Mach Number	Reynold's Number (based on model length)	Dynamic Pressure lbs/ft^2	ρV lb sec/ft^3	Maximum Side Force Measured (Y max)lbs 600 °/sec	Maximum Yawing Moments Measured (Ψ max) in-lbs 600 °/sec	(pd/2V) at 600 °/sec
.291	2.21×10^6	116.6	0.724	1.39	2.77	1.951
.600	3.88×10^6	405.4	1.253	4.77	10.62	.971
.810	4.44×10^6	606.6	1.427	6.47	14.94	.739
.914	4.56×10^6	690.7	1.463	7.25	17.38	.666
1.57	3.96×10^6	890.0	1.241	3.52	7.89	.438
1.77	3.29×10^6	827.7	1.069	2.68	5.61	.406
1.90	2.98×10^6	782.7	.969	2.18	4.63	.389
2.22	2.33×10^6	657.7	.750	1.10	2.46	.358
2.46	1.95×10	563.5	.610	.91	2.05	.340

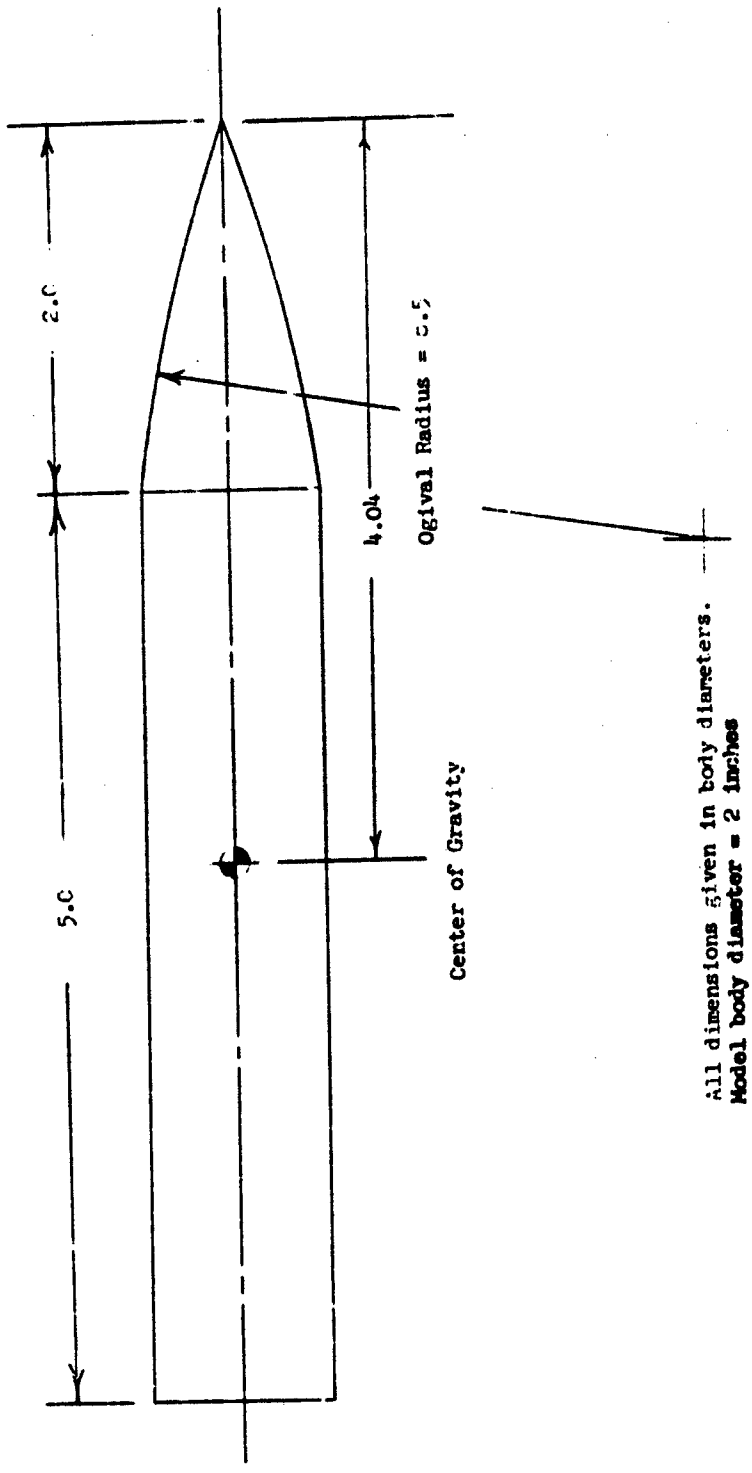
2.0
4.04
Ogival Radius = 5.5
5.0
Center of Gravity
All dimensions given in body diameters.
Model body diameter = 2 inches

SKETCH OF THE 7-CALIBER AN SPINNER MODEL AND SUPPORT SYSTEM

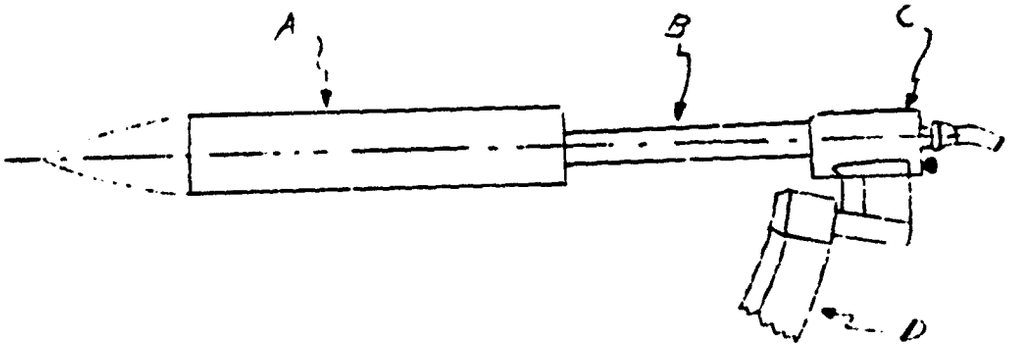

A - 7-Caliber AN Spinner Model (See Figure 3)

B - Sting and Strain-Gage Balance (See Figure 4)

C - Zero-Yaw Device (See Figure 5)

D - Sector

SCHEMATIC SKETCH OF 7-CALIBER AM SPINNER MAGNUS MODEL

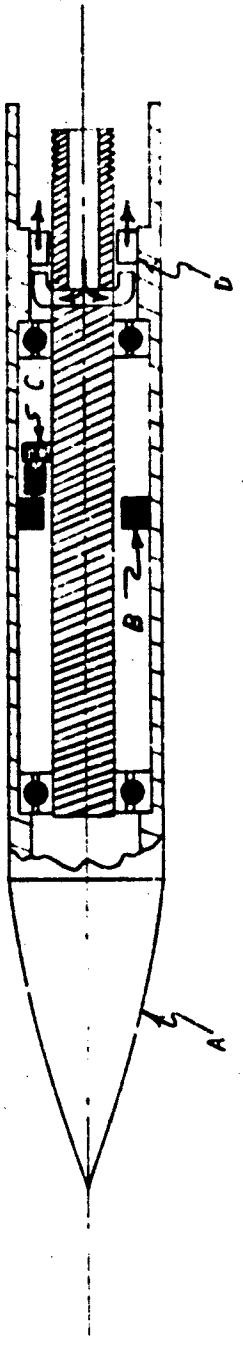

A - Spinning Model Shell

B - Tachometer Magnet

C - Tachometer Pick-up Coil

D - Turbine Rotor

SCHEMATIC SKETCH OF STRAIN-GAGED STING

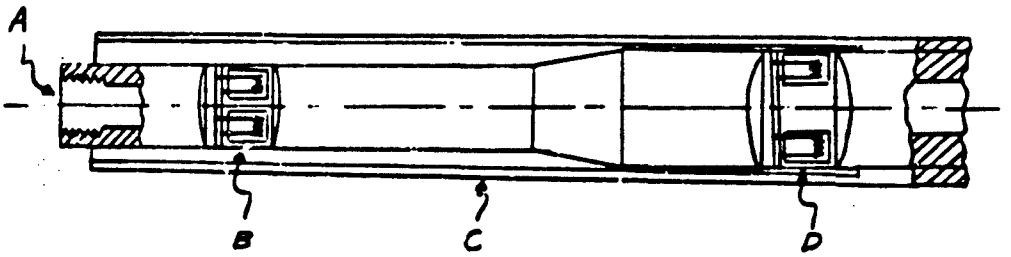

A - Air Passage to Turbine

B - Forward Yaw Gage Section

C - Windshield

D - Aft Yaw Gage Section

ZERO-YAW DEVICE

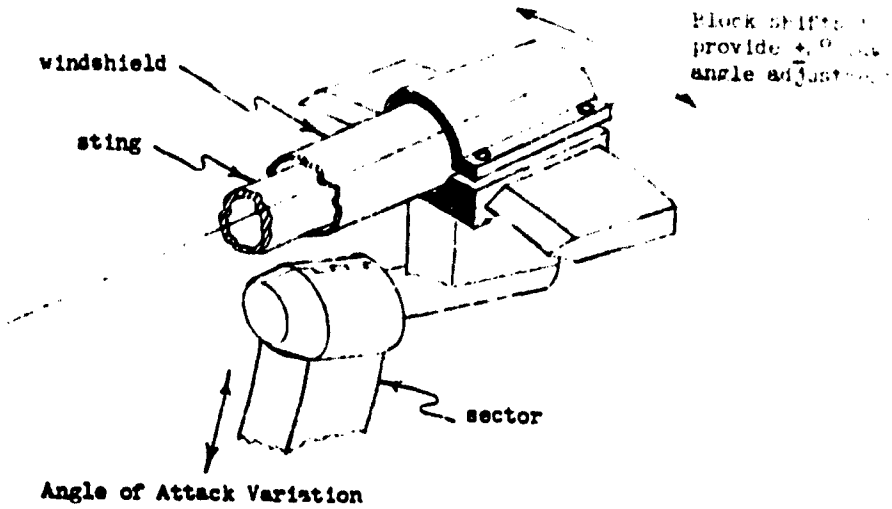

Block shifts to provide ±, ° angle adjust

TACHOMETER AND STRAIN-GAGE SYSTEMS

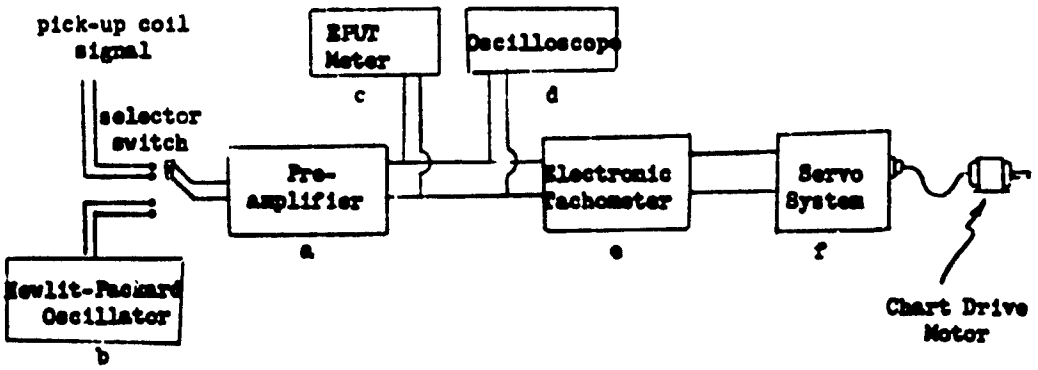

Tachometer System

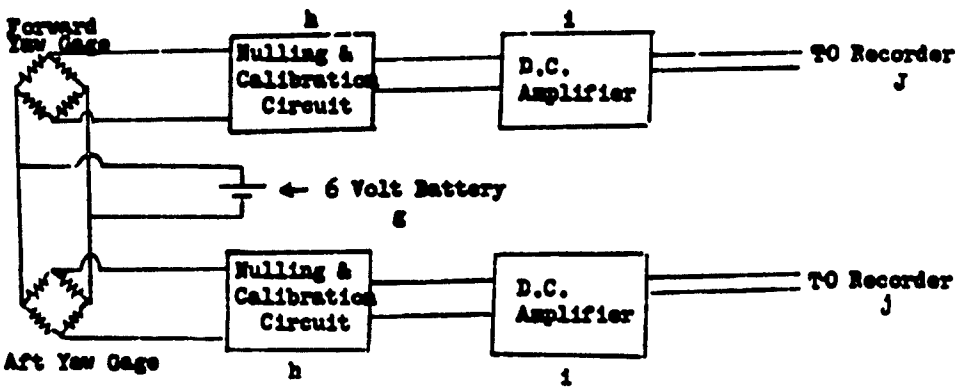

Strain-Gage System

Fig. 6

SCHEMATIC SKETCH OF THE TACHOMETER SERVO SYSTEM
FOR POSITIONING THE RECORDER CHART AS A FUNCTION OF MODEL SPIN RATE

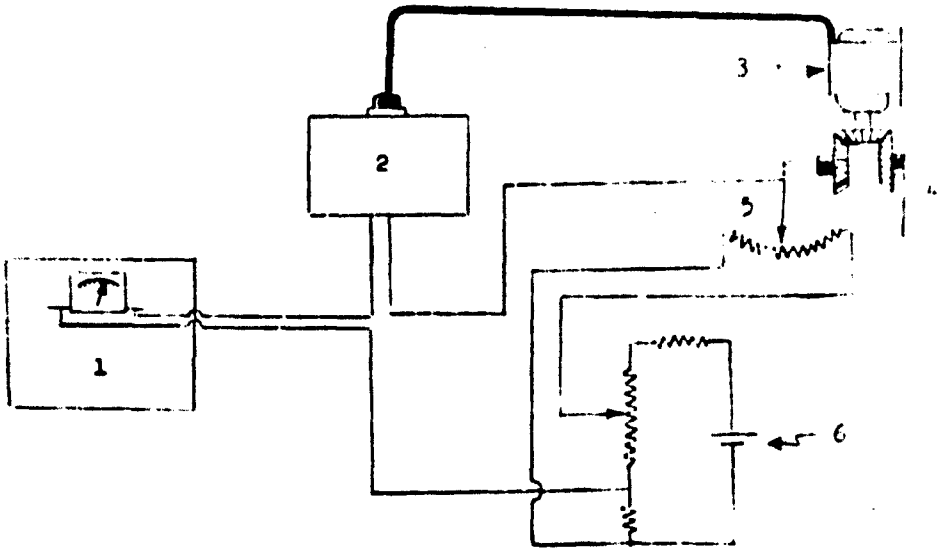

1 - Electronic Tachometer

2 - Servo Amplifier

3 - Servo Motor for Chart Drive

4 - Recorder Chart

5 - Nulling Helipot

6 - 1 1/2 Volt Battery

Fig. 7

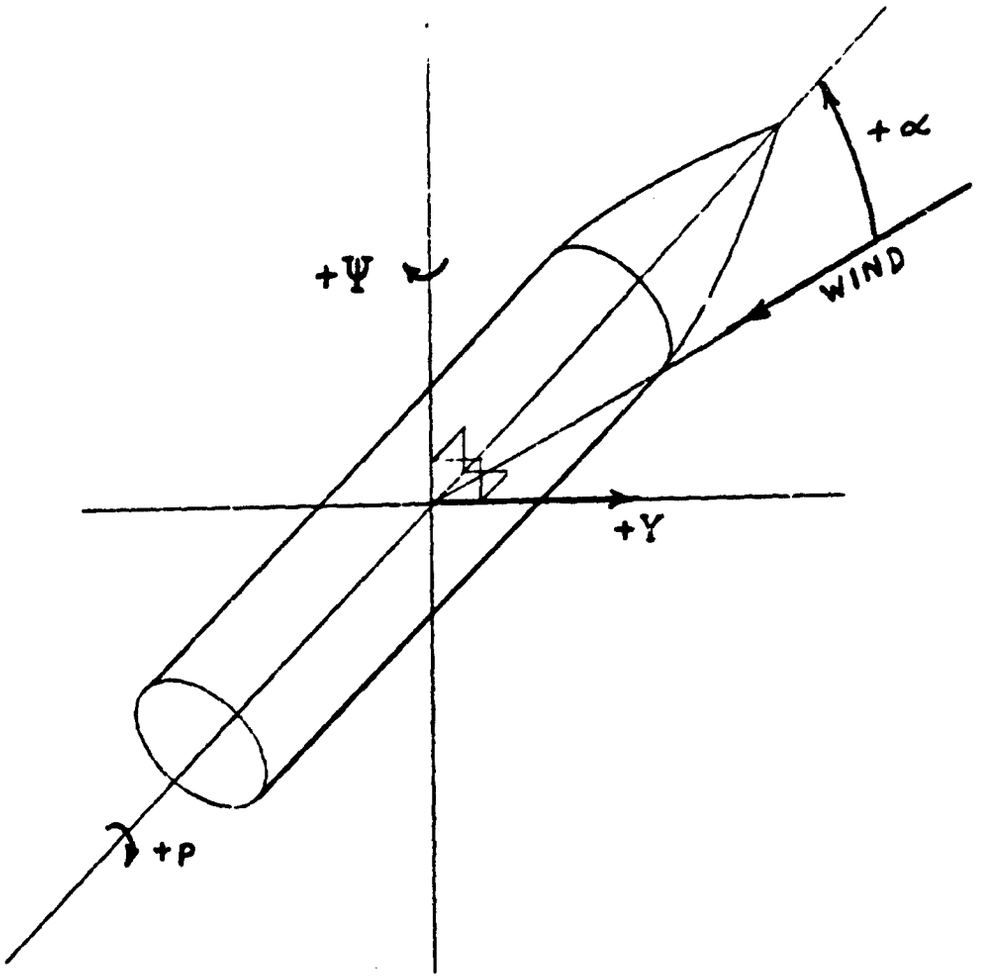

Wind-Tunnel Force and Moment Coordinate System

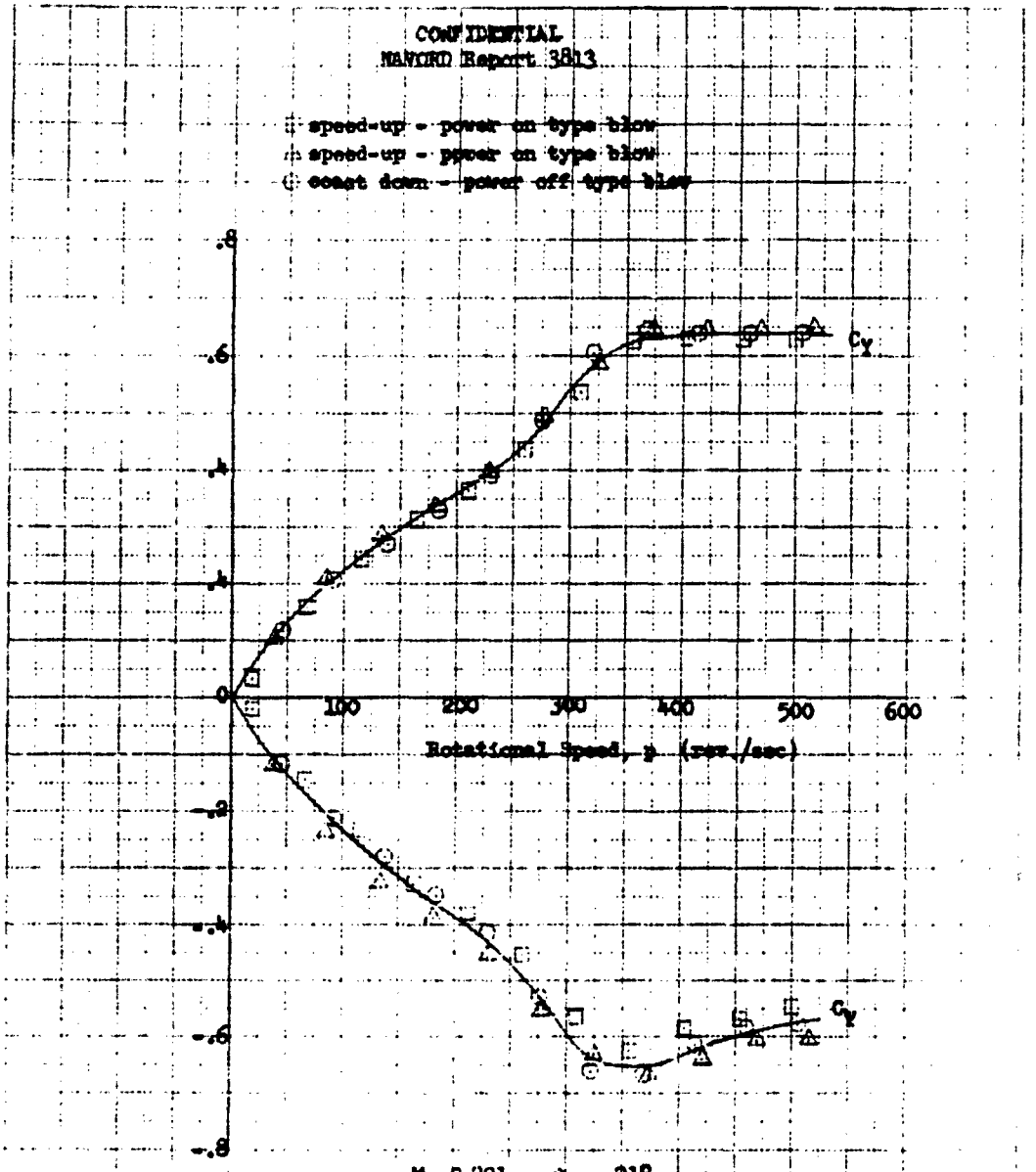

Comparison of Data obtained during Speed up Type Flows and a Coast down Type Flow

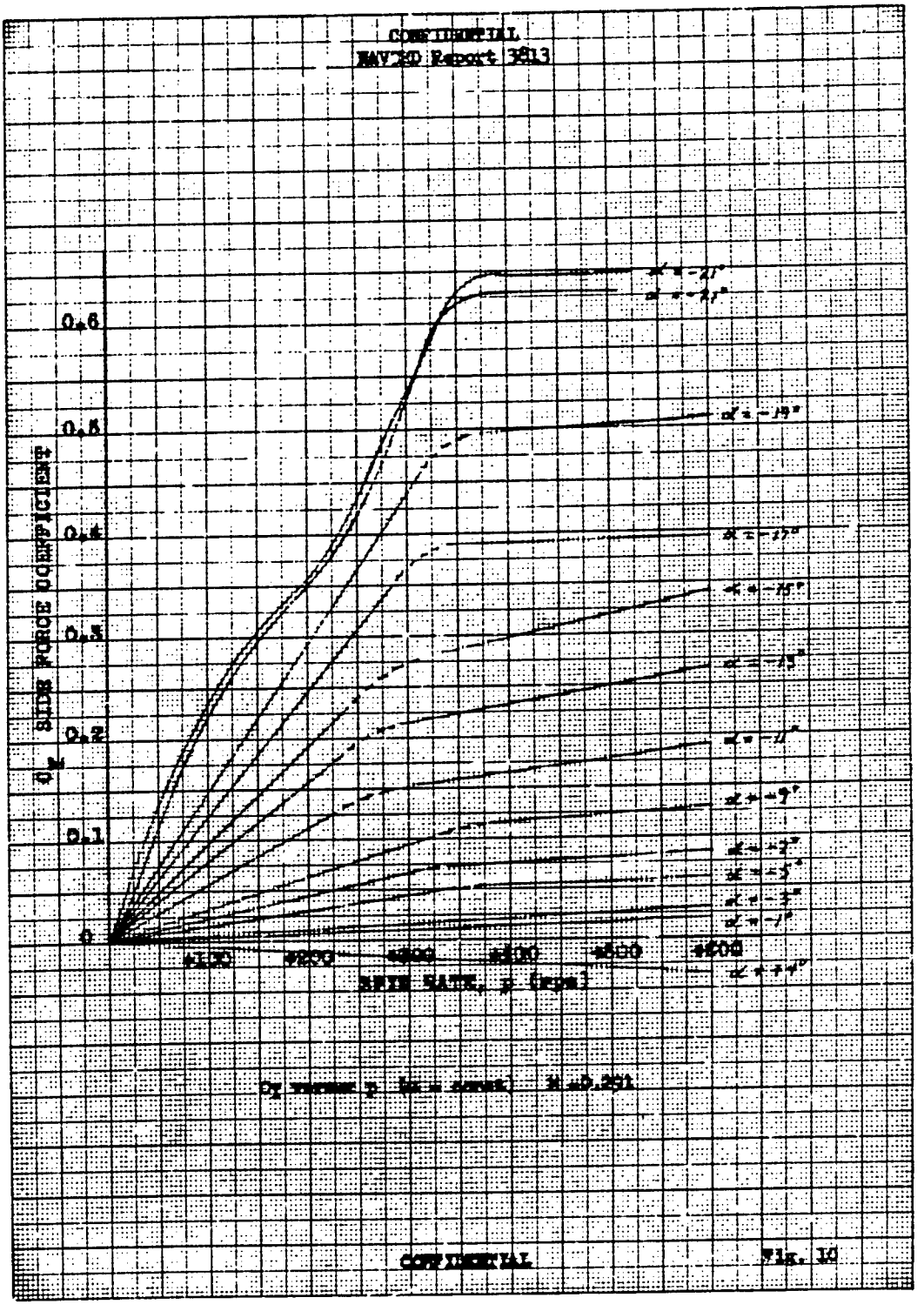

CONFIDENTIAL

Fig. 10

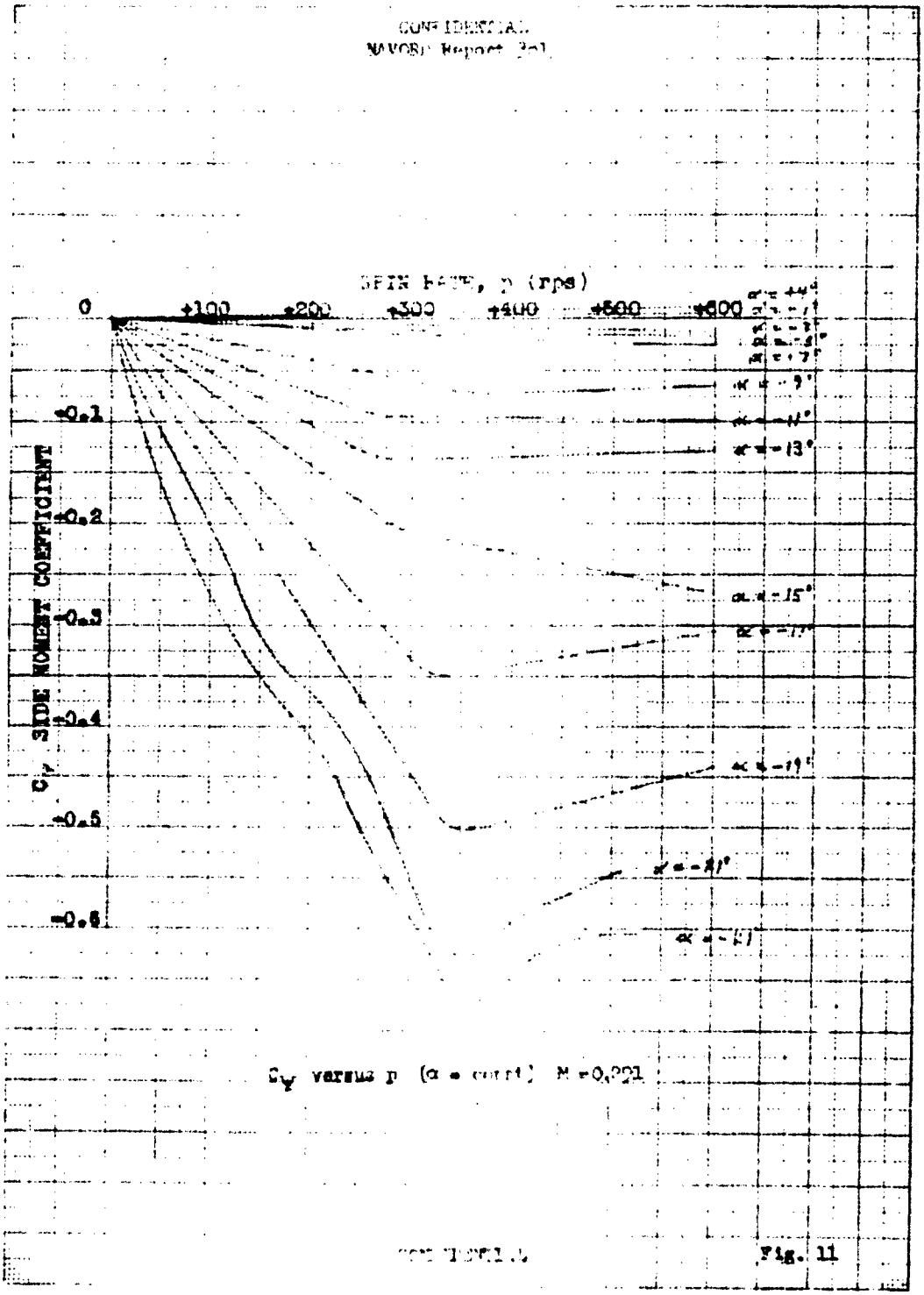

C_{l_p} versus p (α = curve) M = 0.901

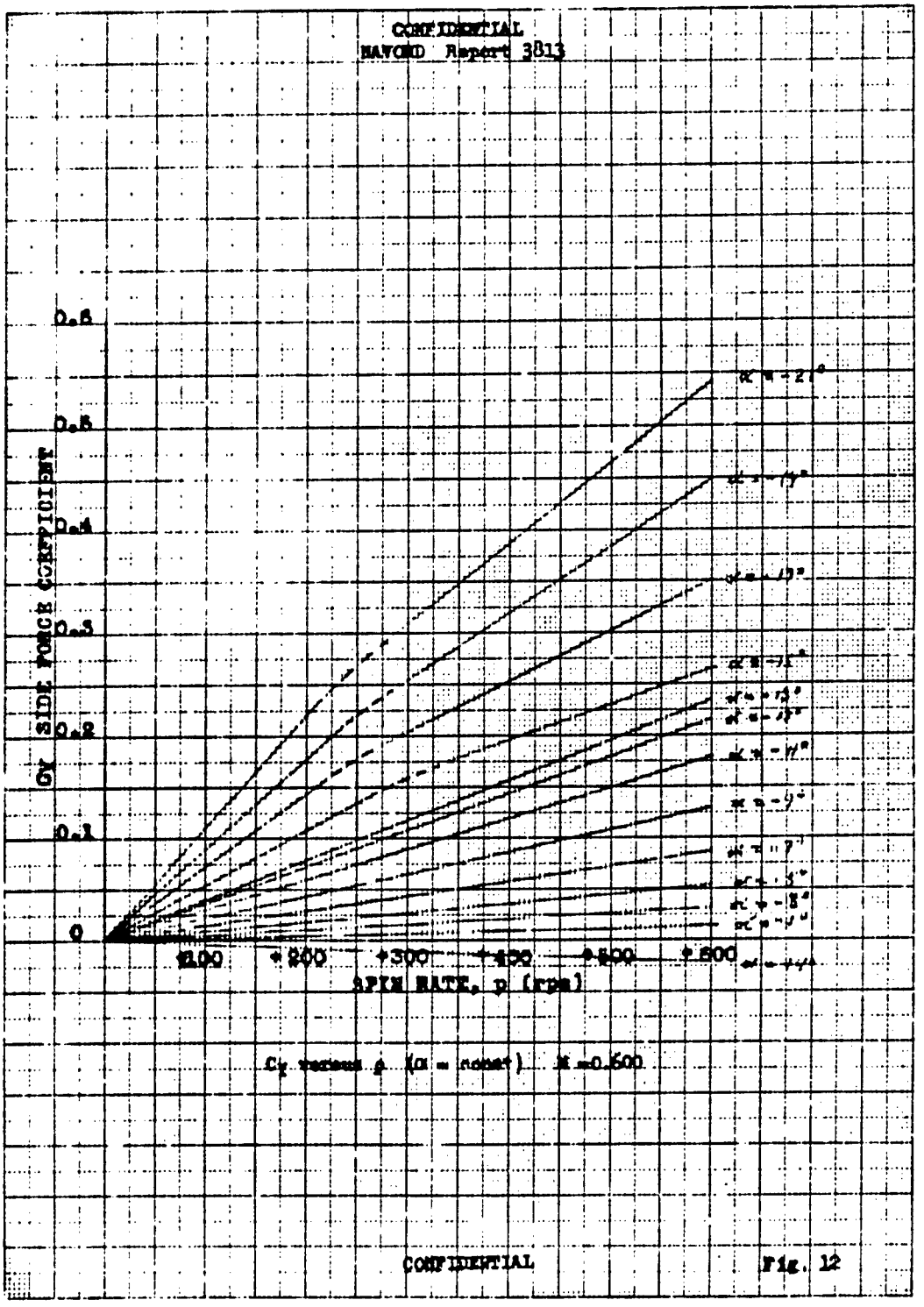

C_y versus p (α = const) $M = 0.600$

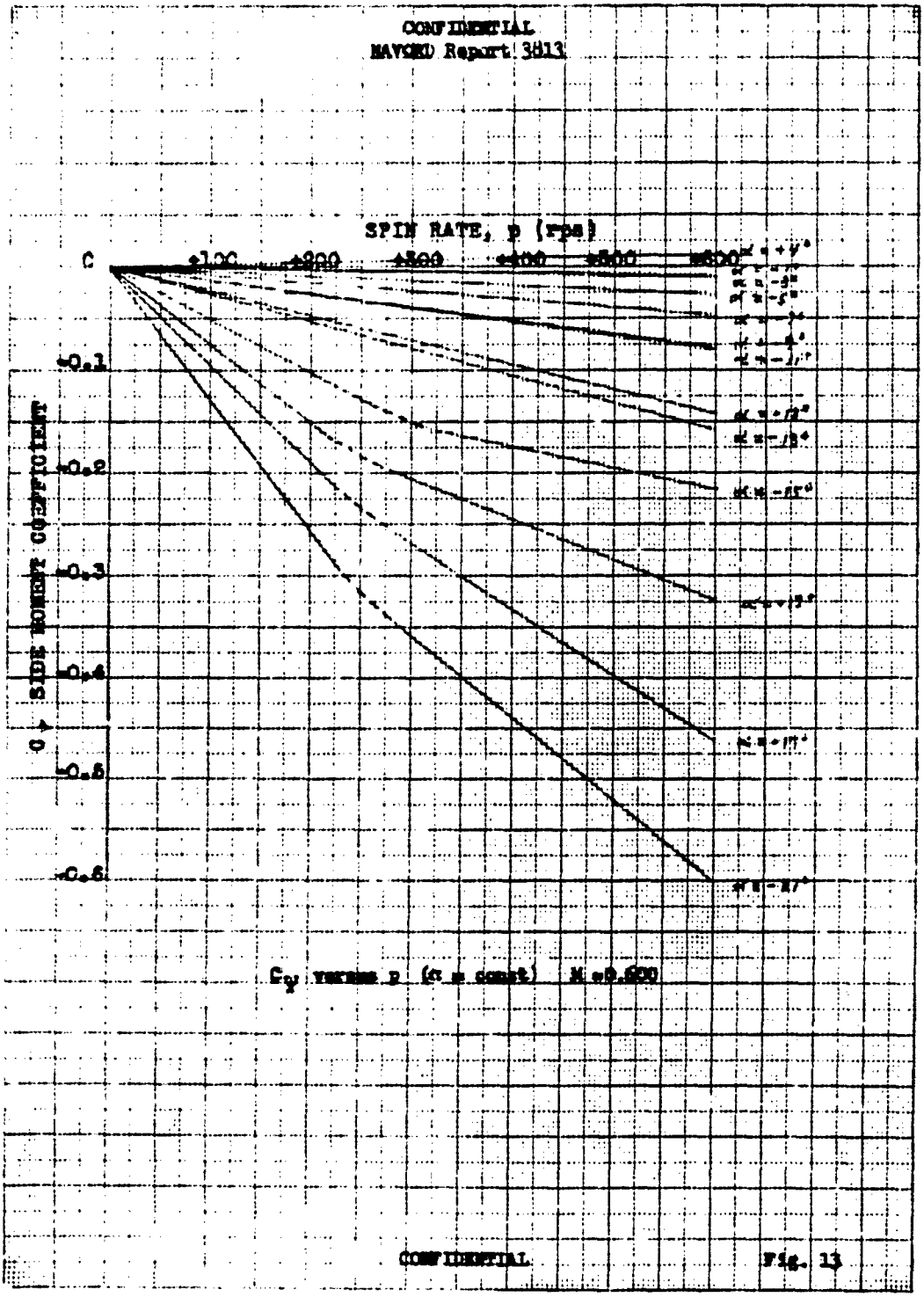

C_y versus p (α = const) M=0.600

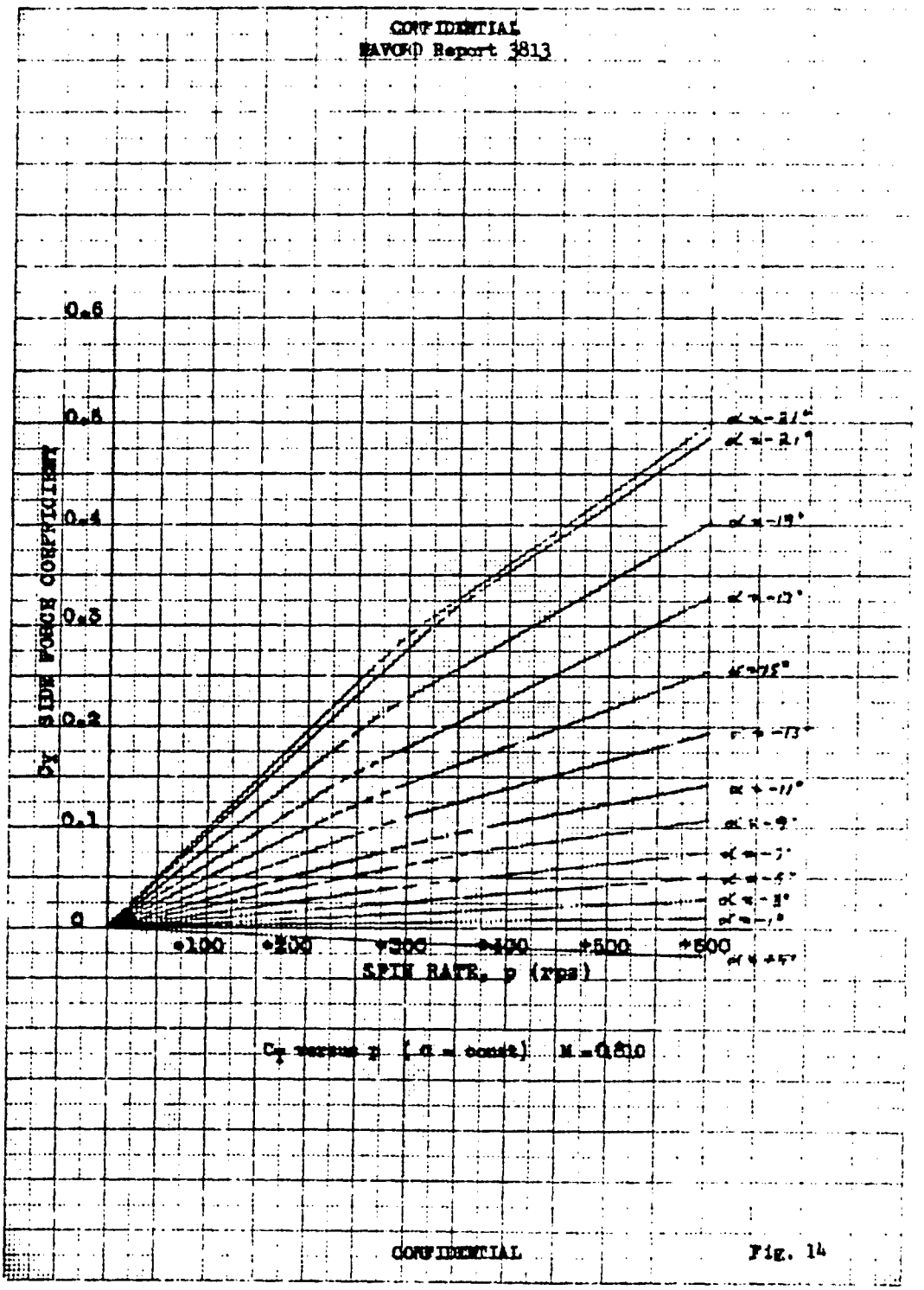
0.6
0.5
0.4
0.3
0.2
0.1
0
C_Y SIDE FORCE COEFFICIENT
+100
+200
+300
+400
+500
+600
SPIN RATE, p (rps)
C_Y versus p (α = const) M = 0.810

Fig. 14

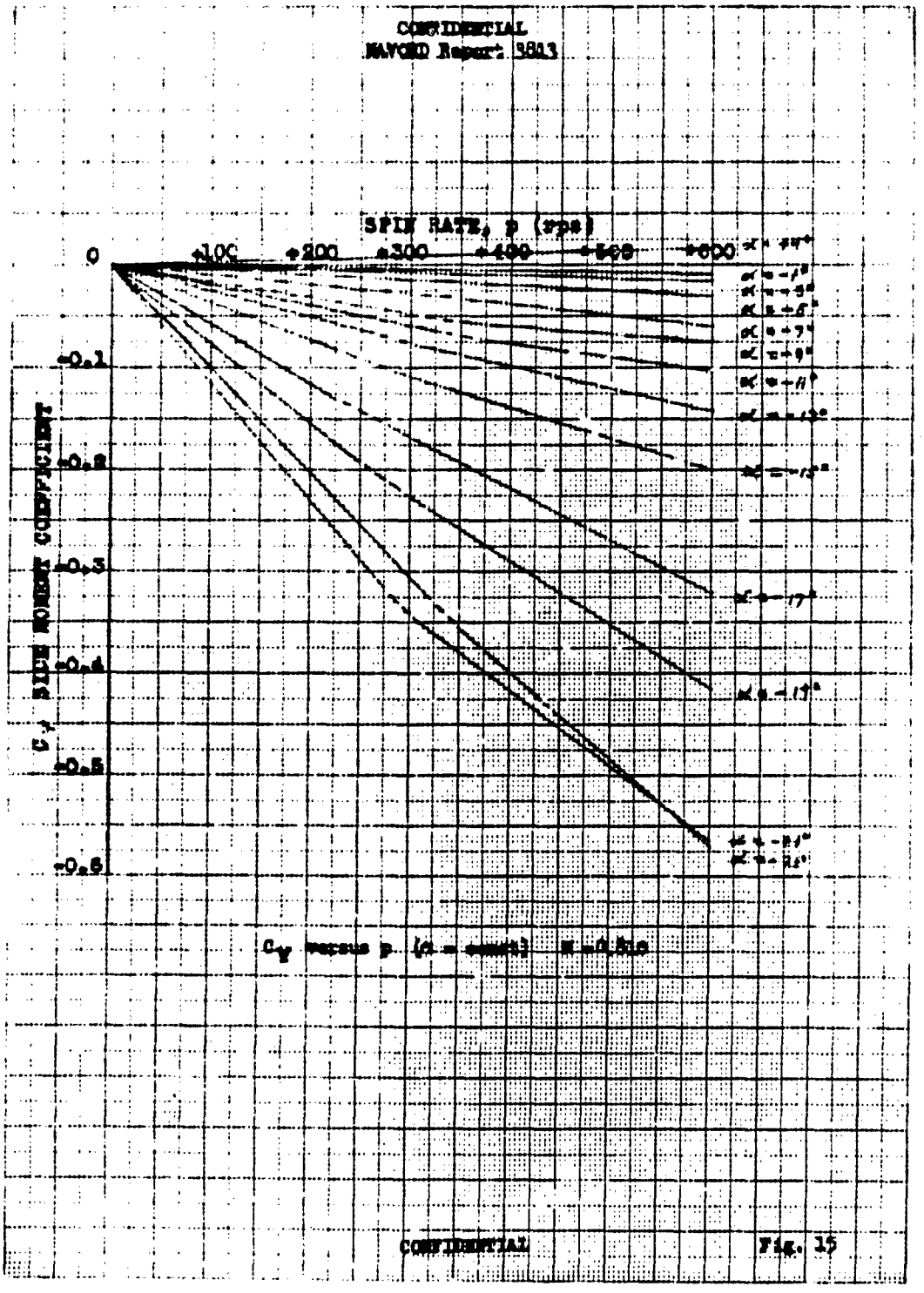

CONFIDENTIAL

Fig. 15

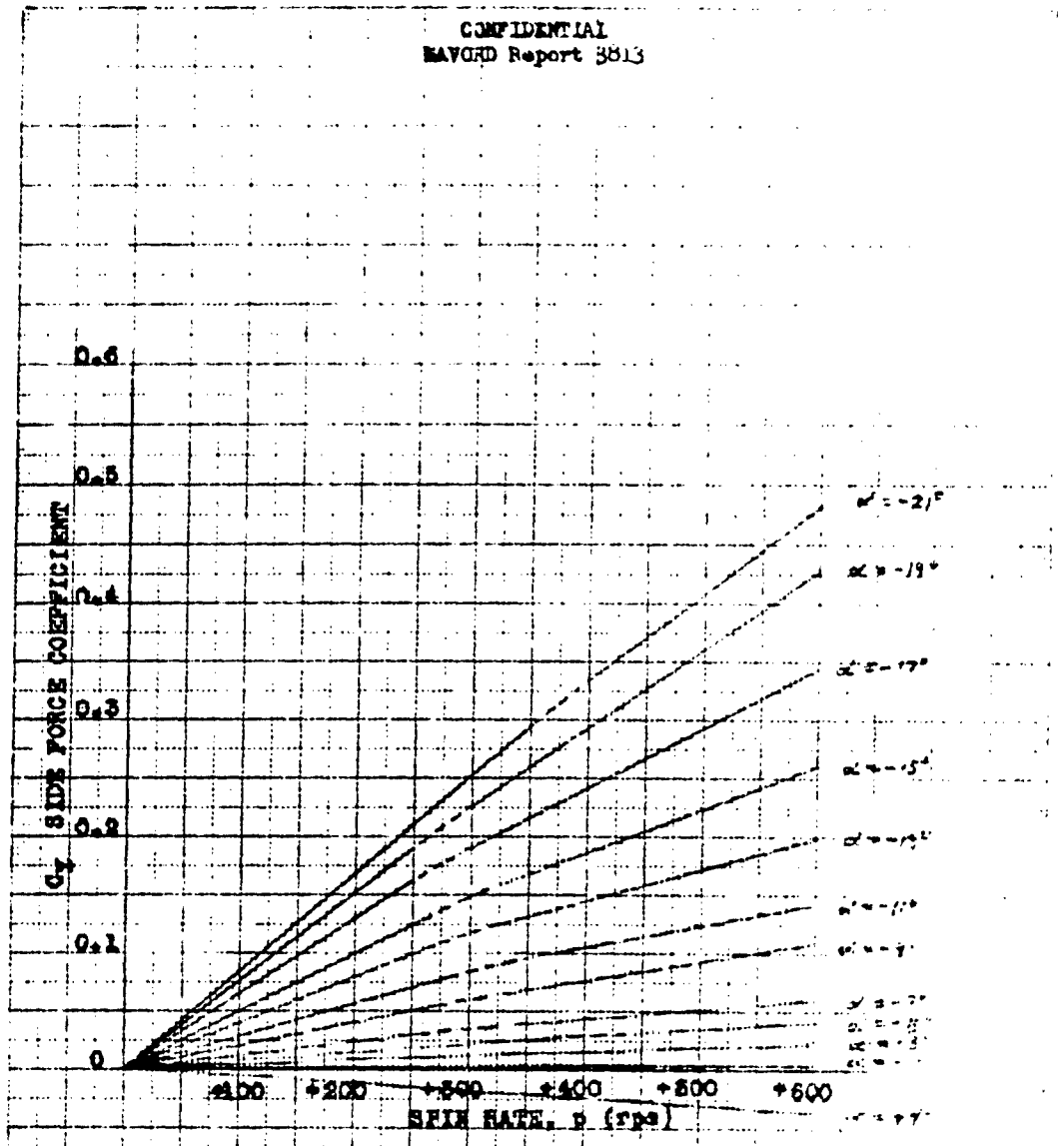

C_Y versus p (α = const) M = 0.914

Fig. 16

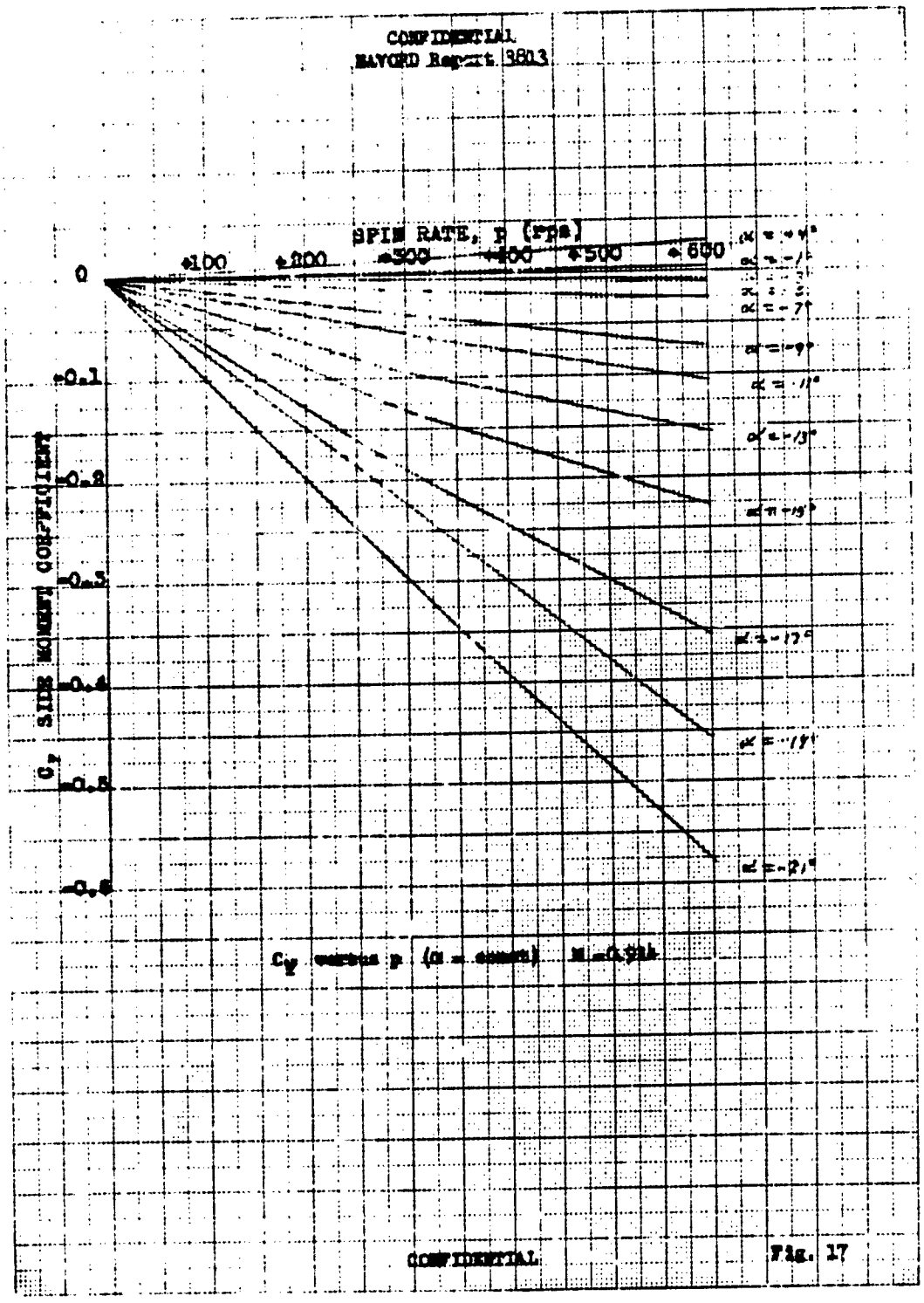
SPIN RATE, p (rps)
+100
+200
+300
+400
+500
+600
0
-0.1
-0.2
-0.3
-0.4
-0.5
-0.6
SIDE MOMENT COEFFICIENT
C_y
$\alpha = +4°$
$\alpha = -7°$
$\alpha = -9°$
$\alpha = -11°$
$\alpha = -13°$
$\alpha = -15°$
$\alpha = -17°$
$\alpha = -19°$
$\alpha = -21°$
C_y versus p (α = constant) M = 0.95

Fig. 17

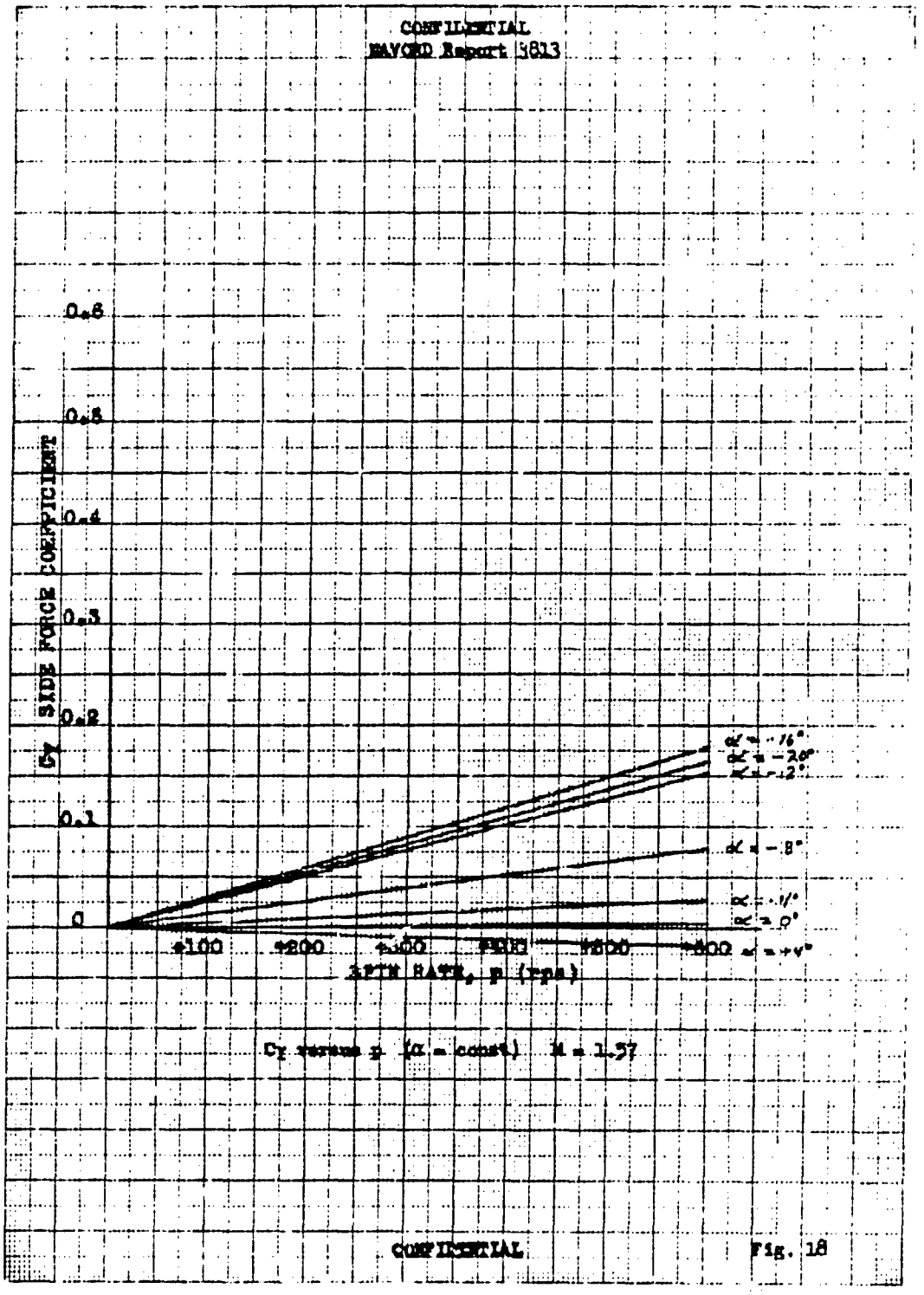

C_Y versus p (α = const.) M = 1.57

Fig. 18

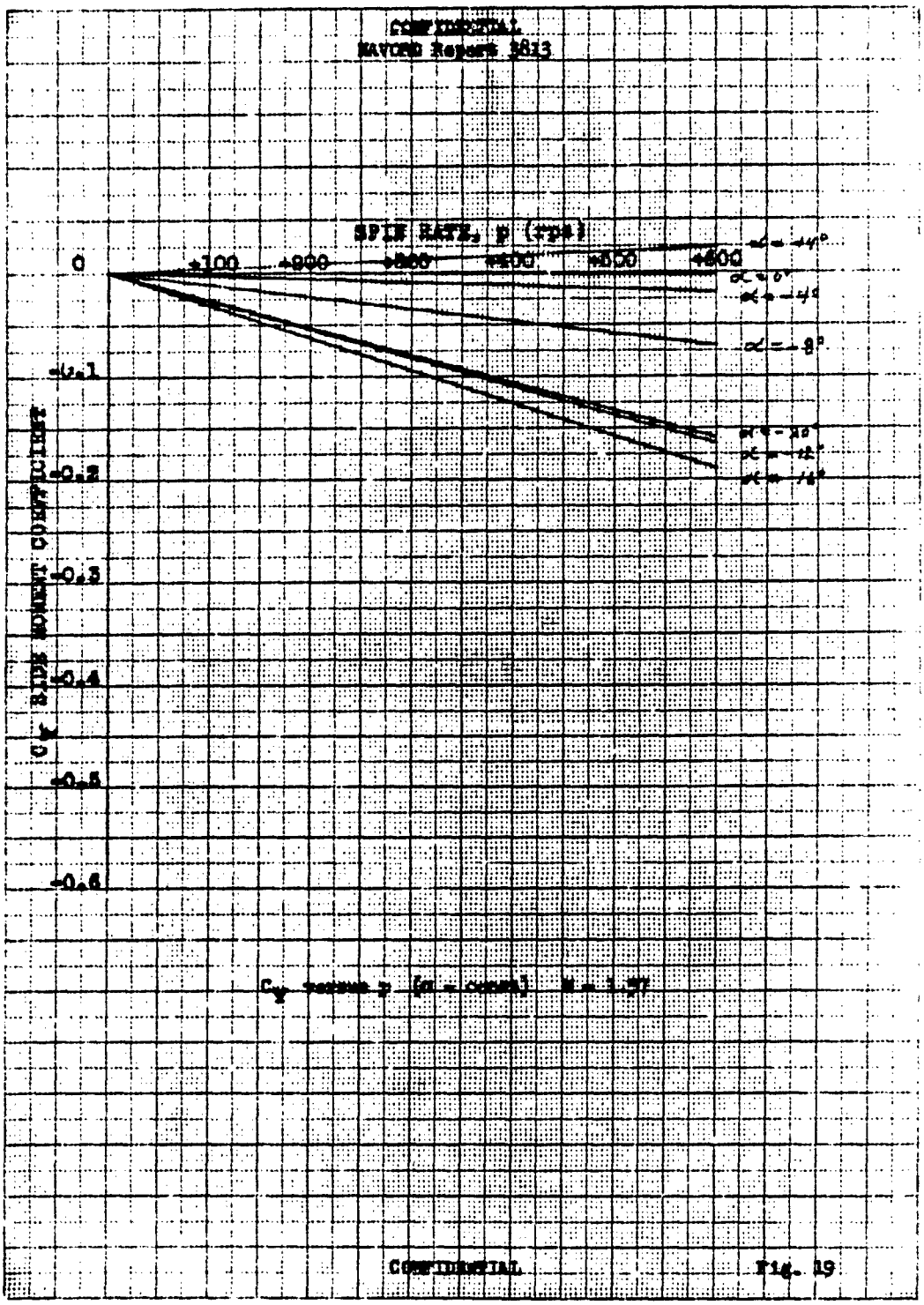
SPIN RATE, p (rps)
0
+100
+200
+300
+400
+500
+600
$\alpha = +4°$
$\alpha = 0°$
$\alpha = -4°$
$\alpha = -8°$
$\alpha = -12°$
$\alpha = -16°$
$\alpha = -20°$
C_{y_p} ROLL MOMENT COEFFICIENT
-0.1
-0.2
-0.3
-0.4
-0.5
-0.6
C_{y_p} versus p (in - cycle) M = 1.97

Fig. 19

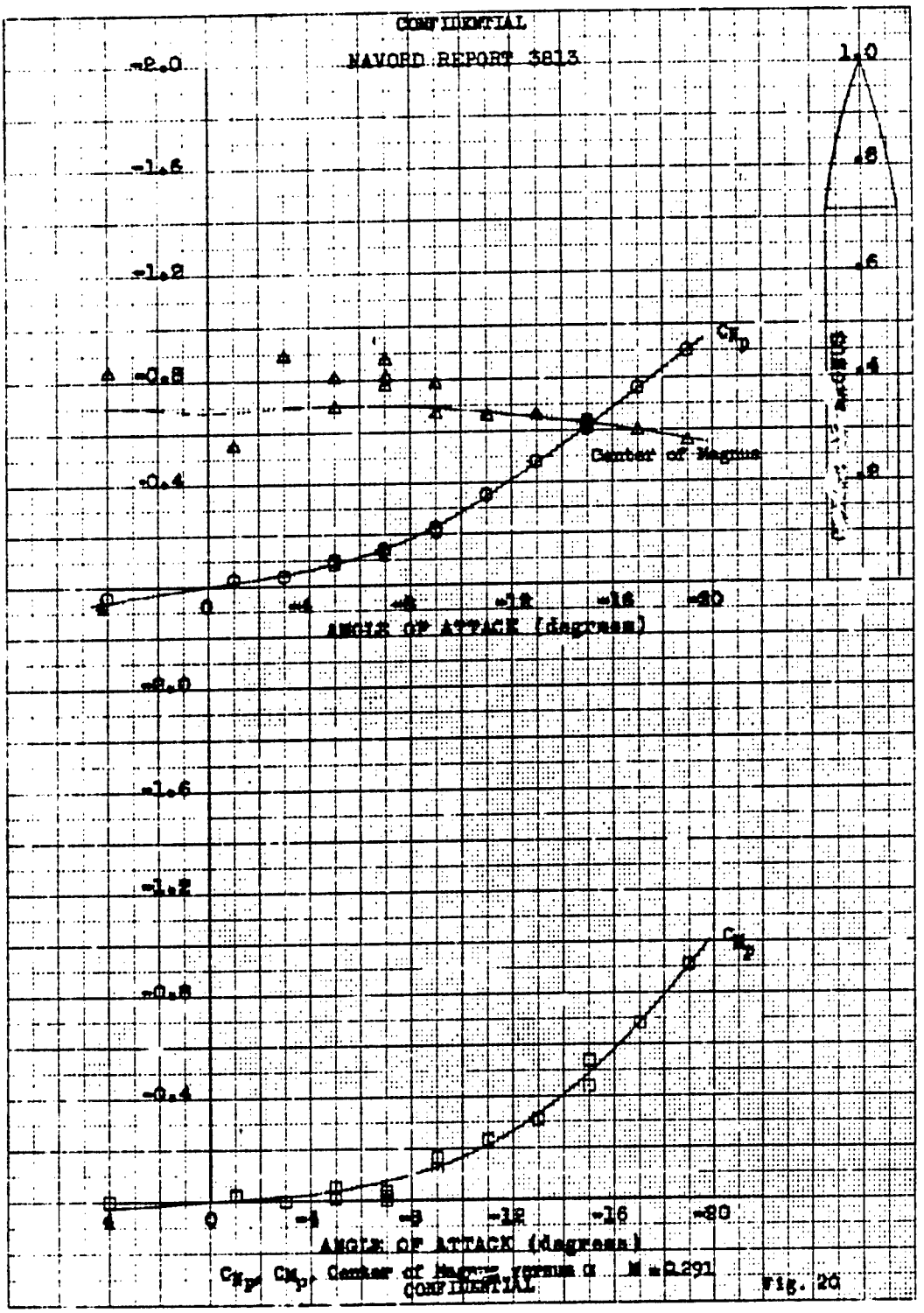

C_{N_p}, C_{M_p}, Center of Magnus versus α M = 2.291

Fig. 20

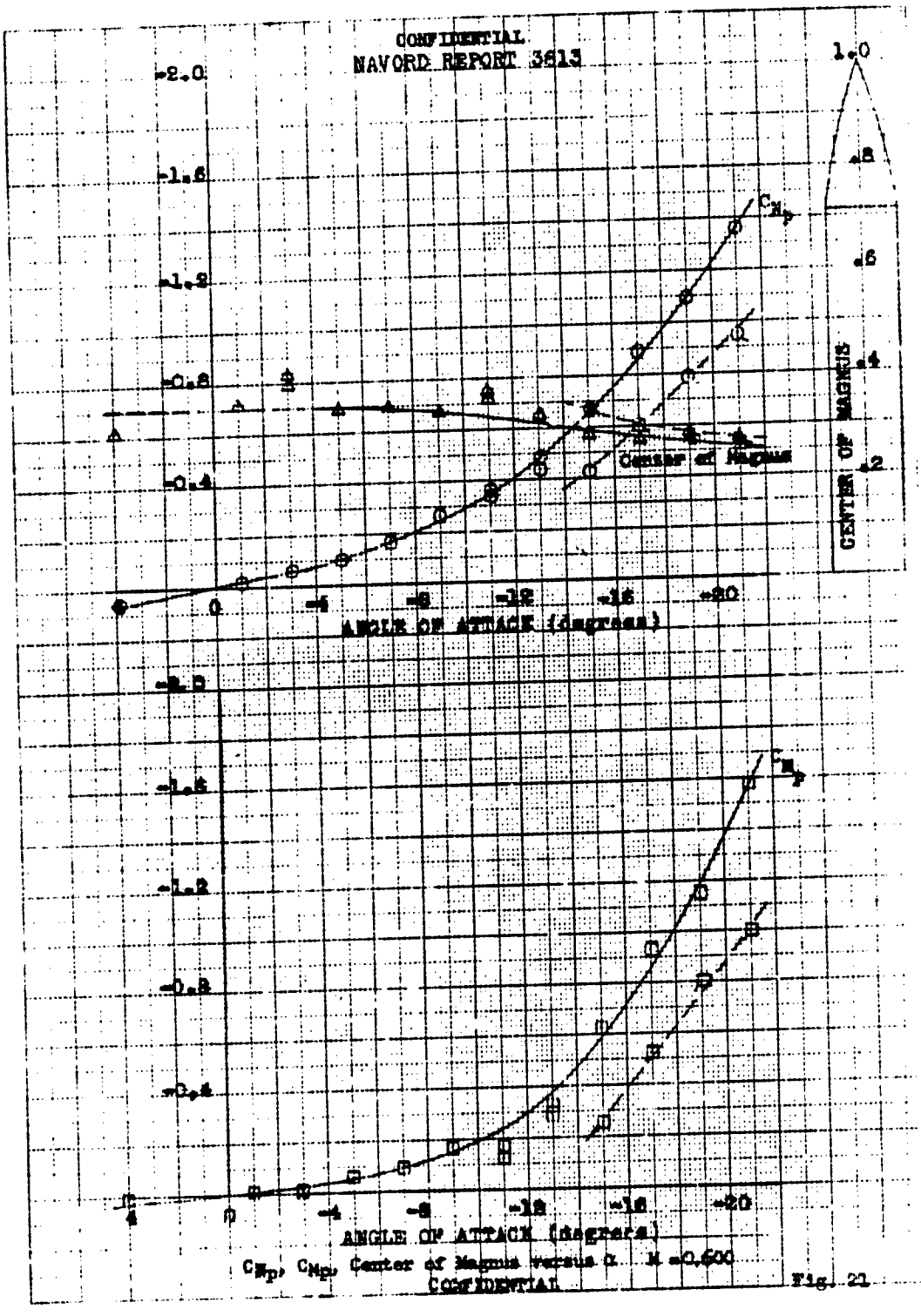

C_{M_p}, C_{N_p}, Center of Magnus versus α. M = 0.600

Fig. 21

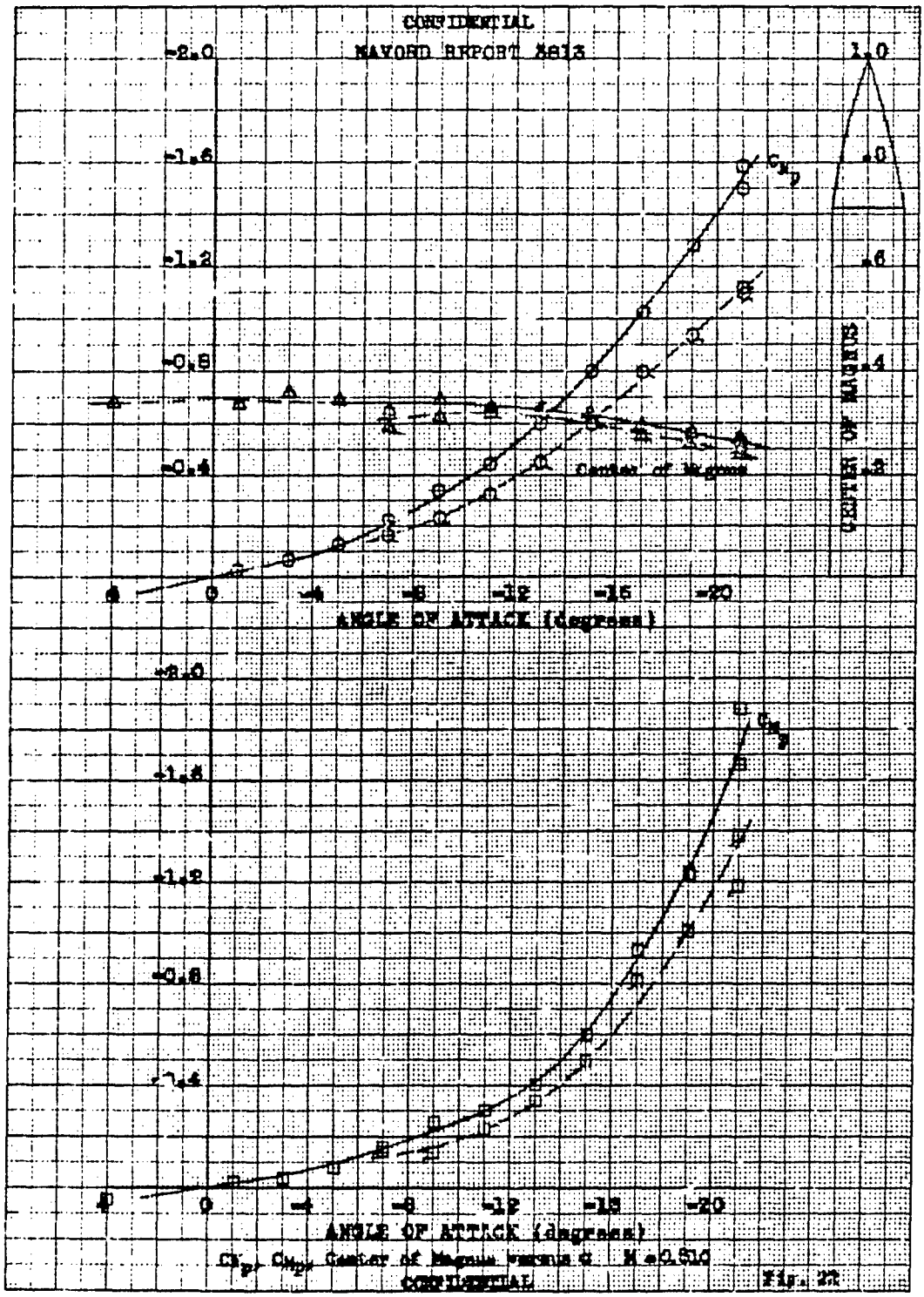

C_{N_p}, C_{M_p} Center of Magnus versus α M = 0.510

CONFIDENTIAL

Fig. 22

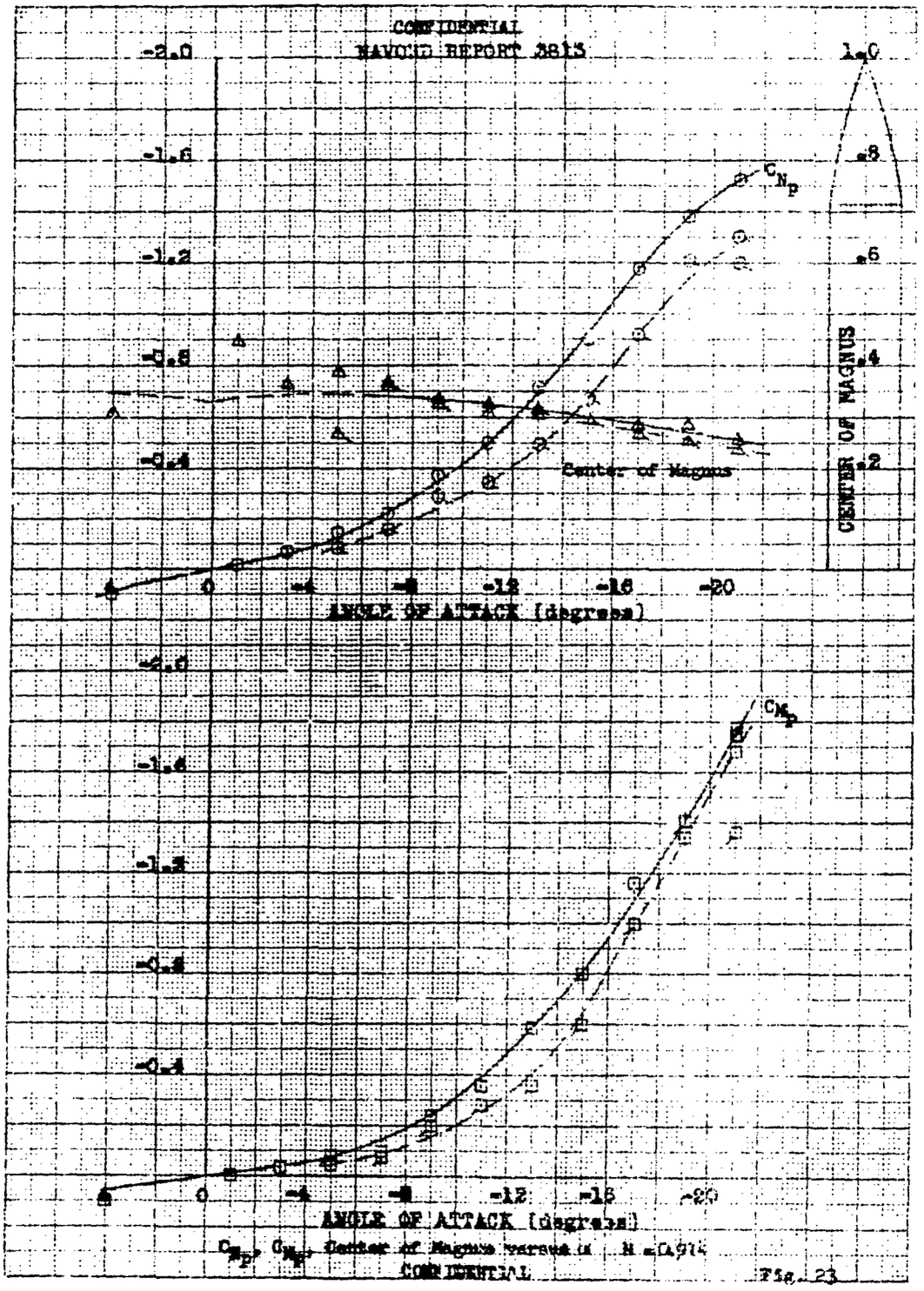

C_{N_p}, C_{M_p}, Center of Magnus versus α M = 1.4914

CONFIDENTIAL

Fig. 23

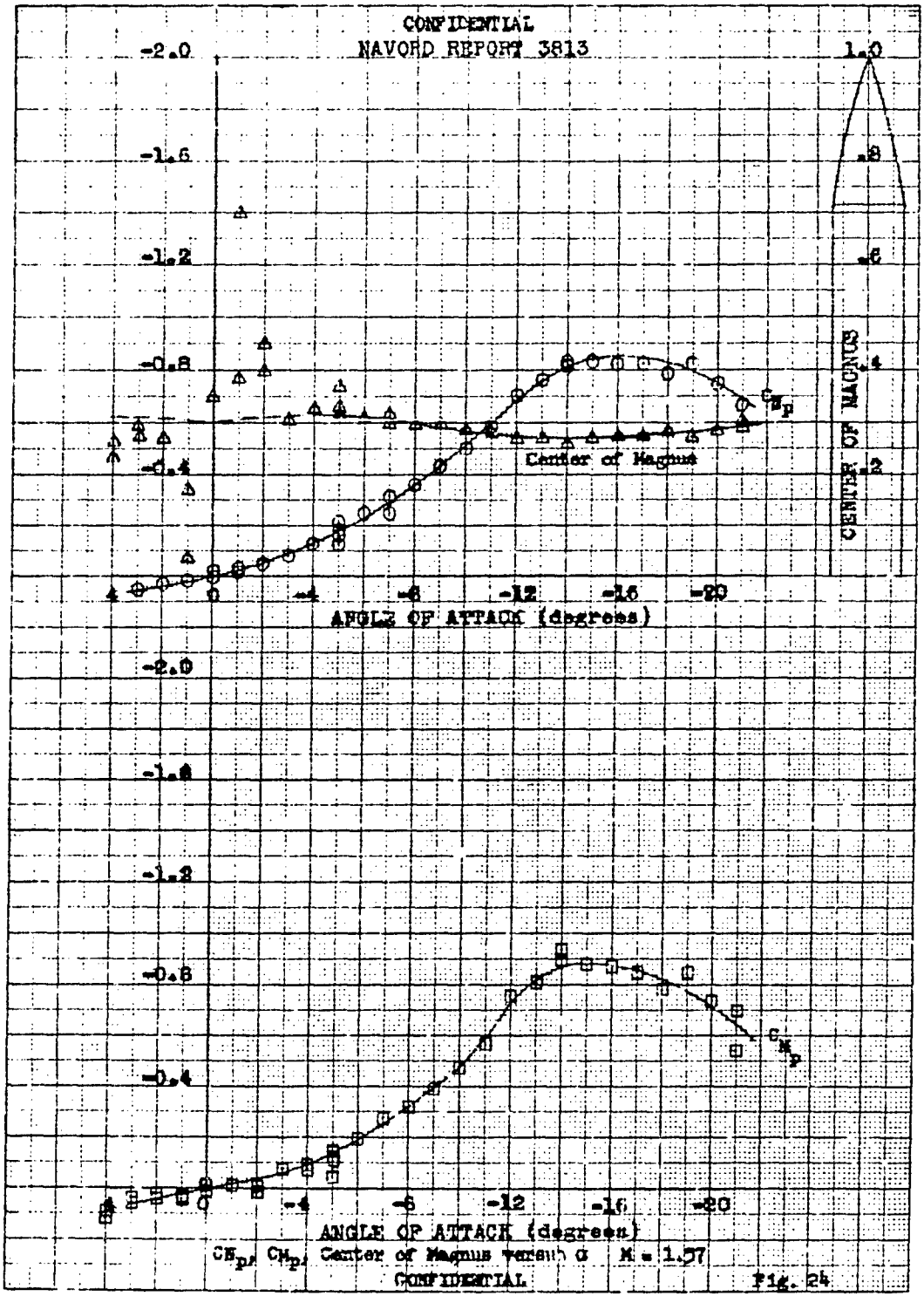

C_{M_p}, C_{M_p}, Center of Magnus versus α M = 1.57

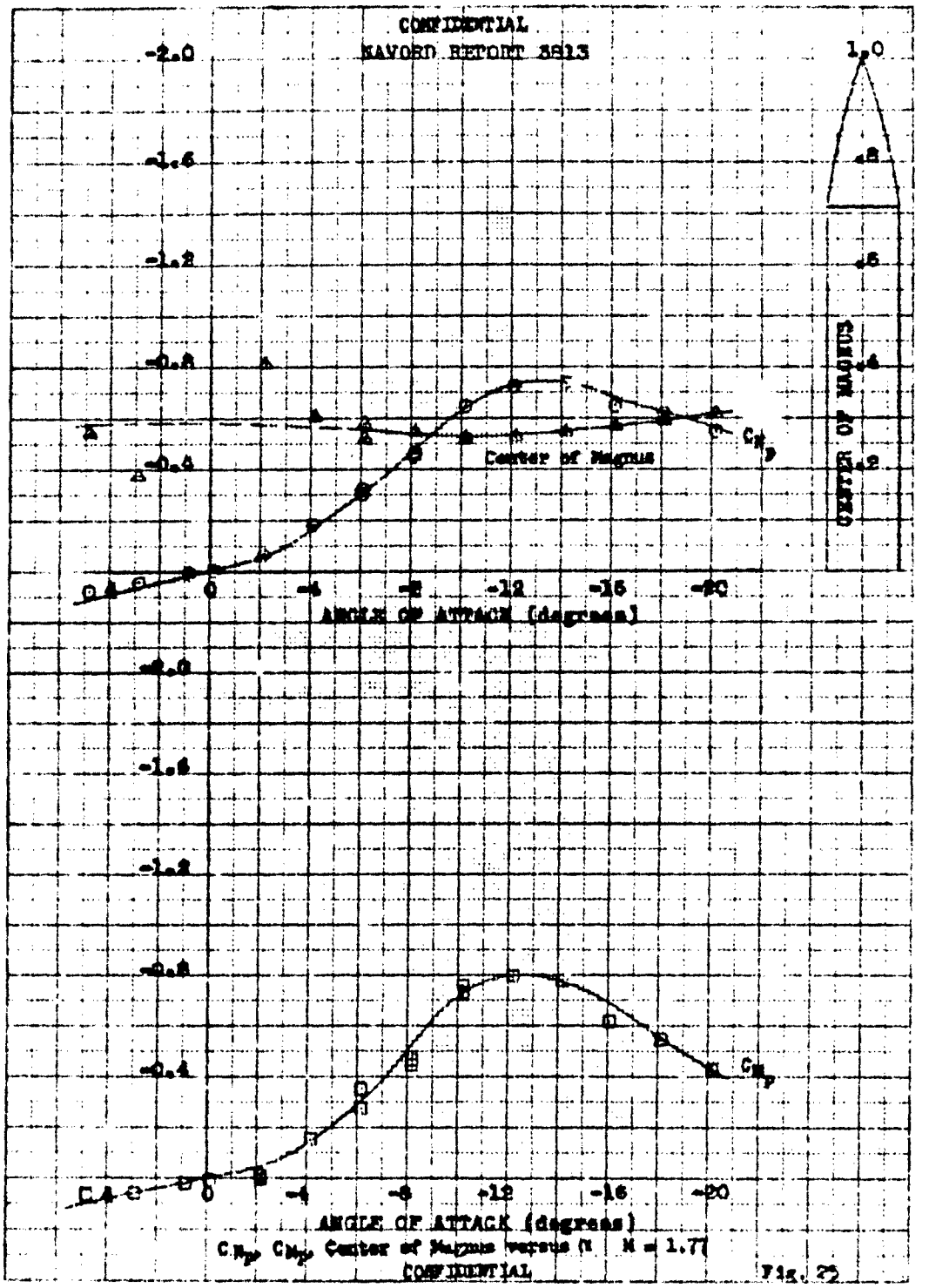

C_{N_p}, C_{M_p}, Center of Magnus versus N M = 1.77

CONFIDENTIAL

Fig. 22

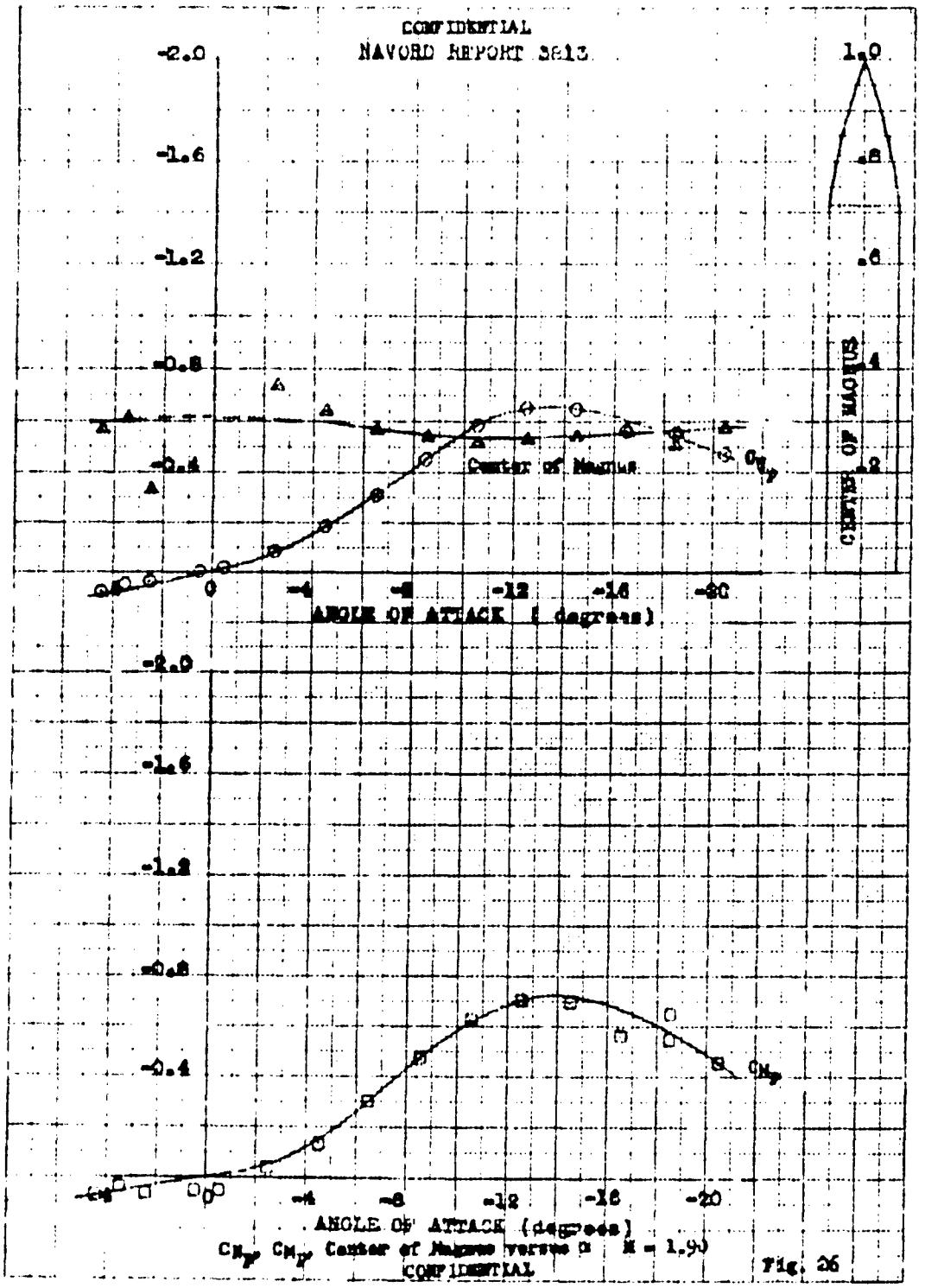

C_{N_p}, C_{M_p}, Center of Pressure versus α M = 1.96

Fig. 26

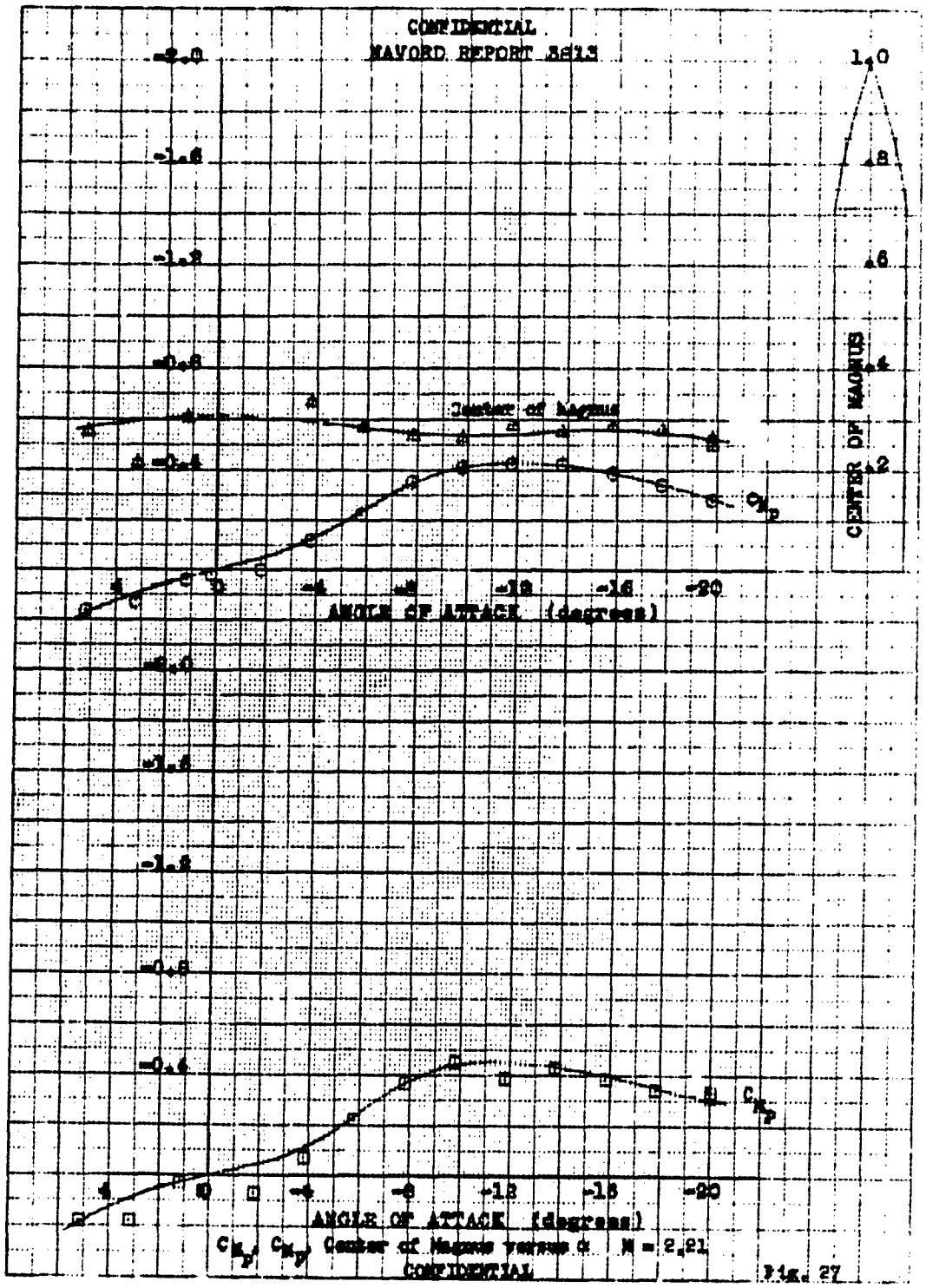

C_{M_p}, C_{M_p} Center of Magnus versus α M = 2.21

CONFIDENTIAL

Fig. 27

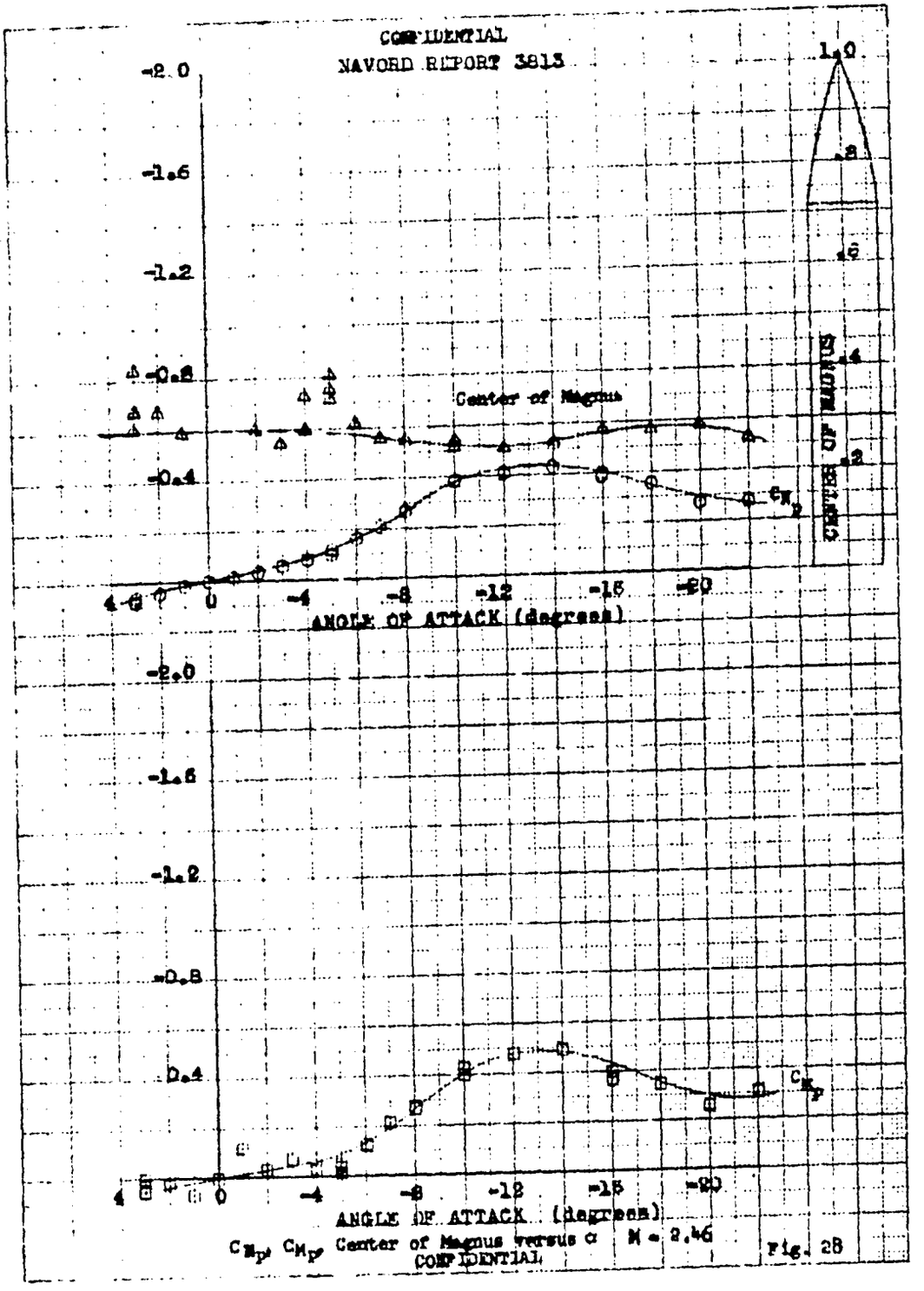

C_{M_p}, C_{M_p} Center of Magnus versus α M = 2.46 Fig. 28

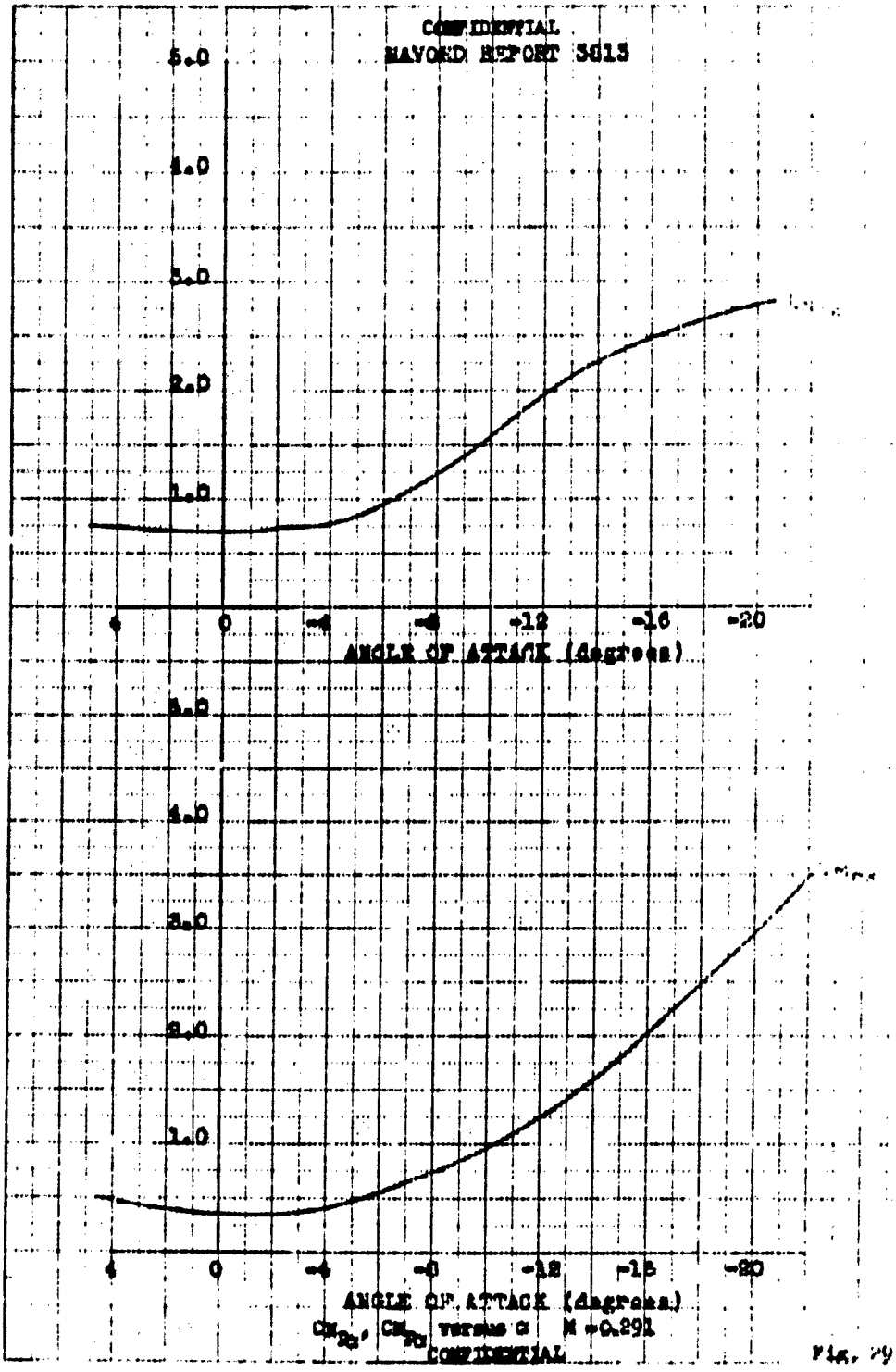

$C_{N_{2\alpha}}$, $C_{N_{3\alpha}}$ versus α M =0.291

Fig. 29

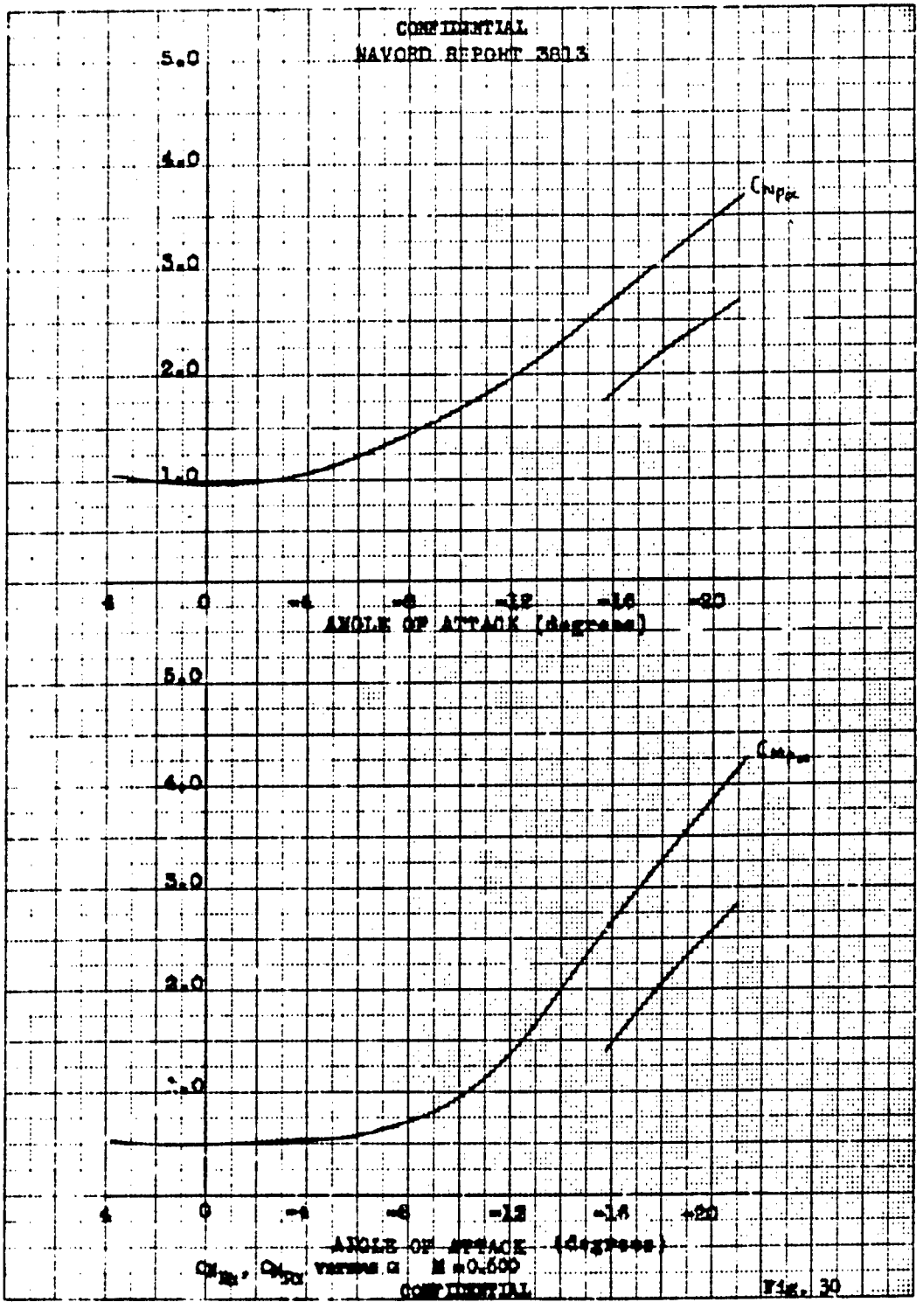

$C_{N_{pt}}$, $C_{m_{pt}}$ versus α M=0.600

CONFIDENTIAL

Fig. 30

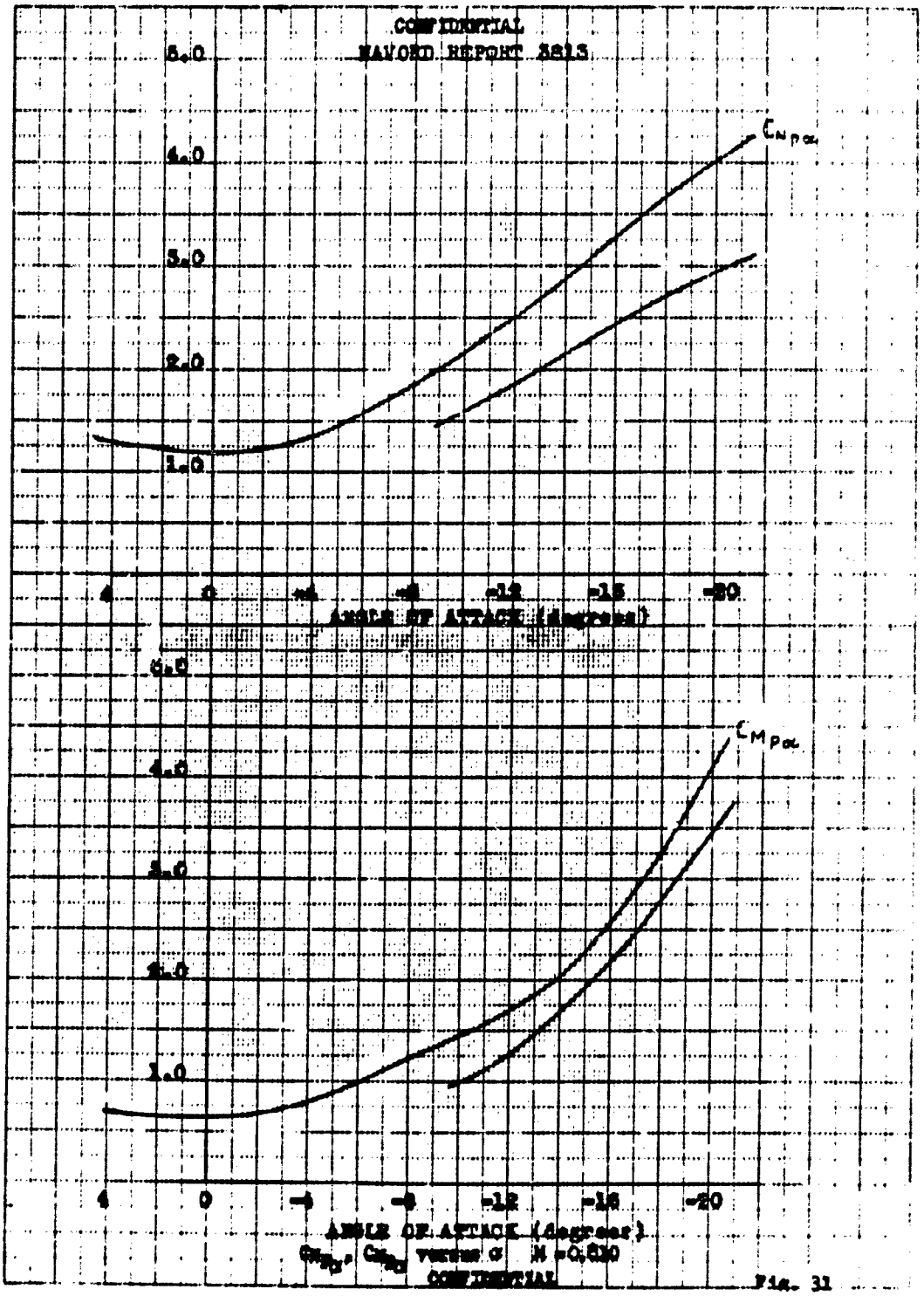

$C_{N_{p\alpha}}$, $C_{M_{p\alpha}}$ versus α M = 0.830

CONFIDENTIAL

Fig. 31

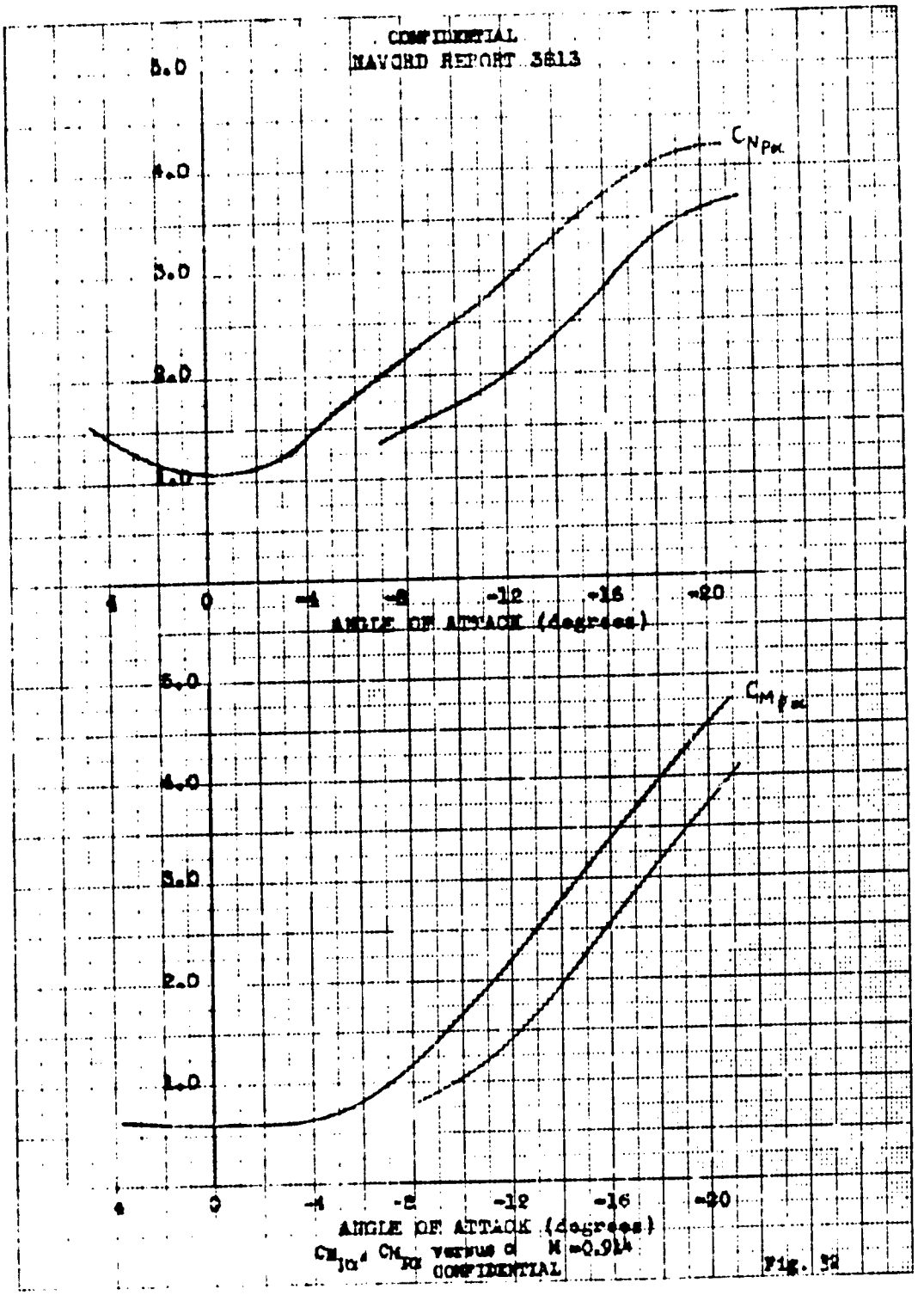

$C_{M_{P\alpha}}$, $C_{M_{P\alpha}}$ versus α M=0.914

CONFIDENTIAL

Fig. 32

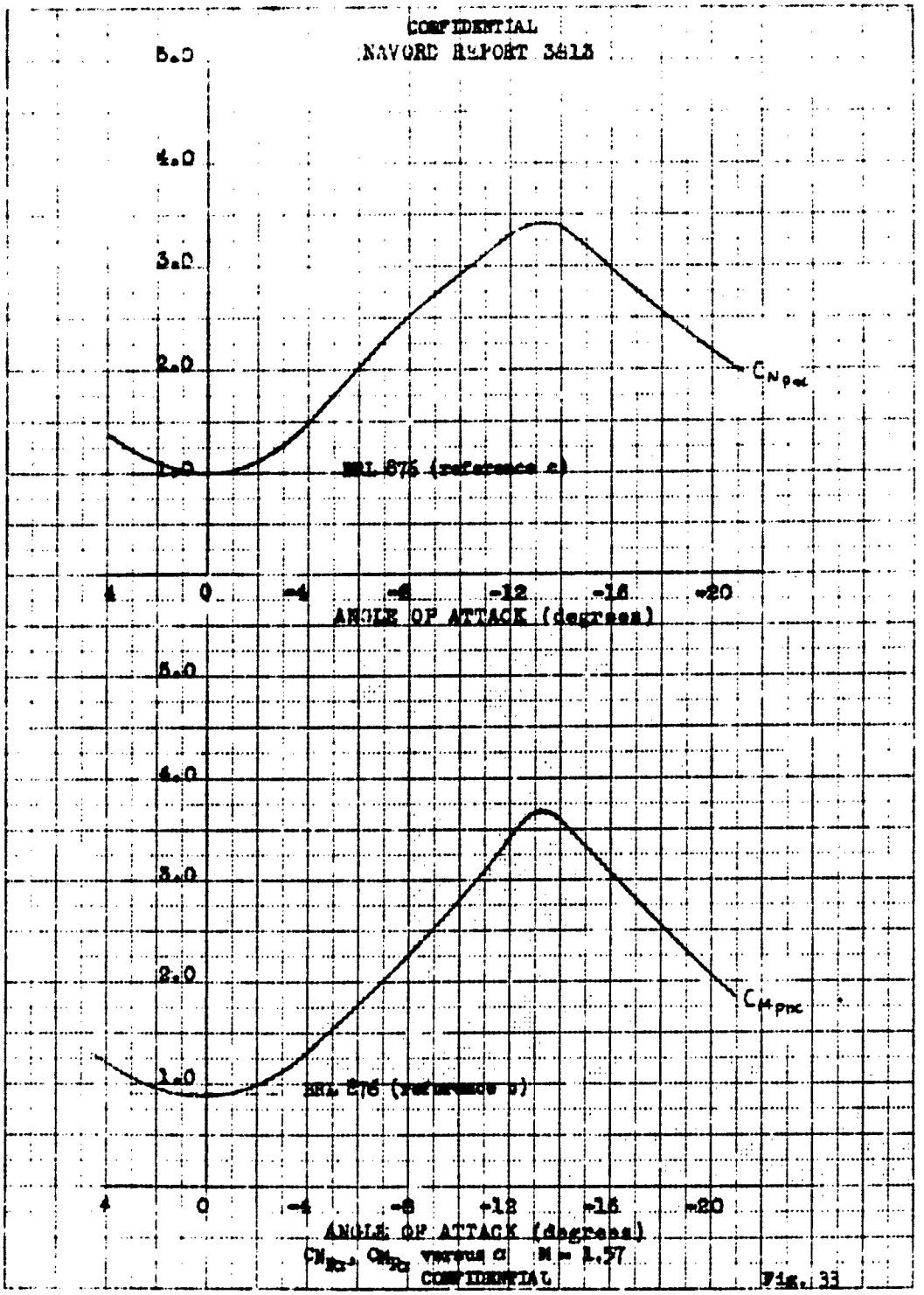

$C_{N_{pc}}$, $C_{M_{pc}}$ versus α M = 1.57

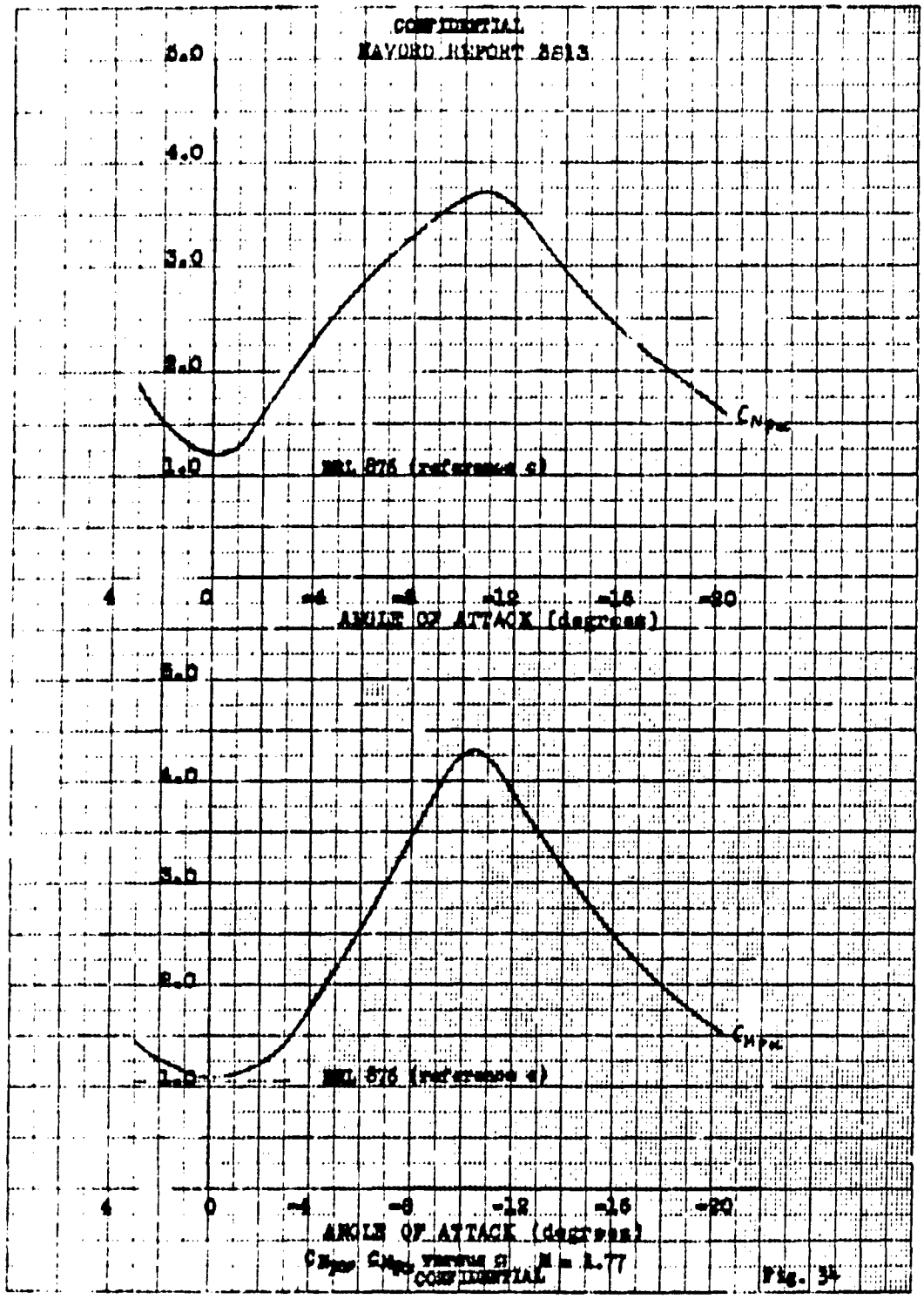

$C_{N_{pc}}$, $C_{M_{pc}}$ versus α, $M = 1.77$

Fig. 34

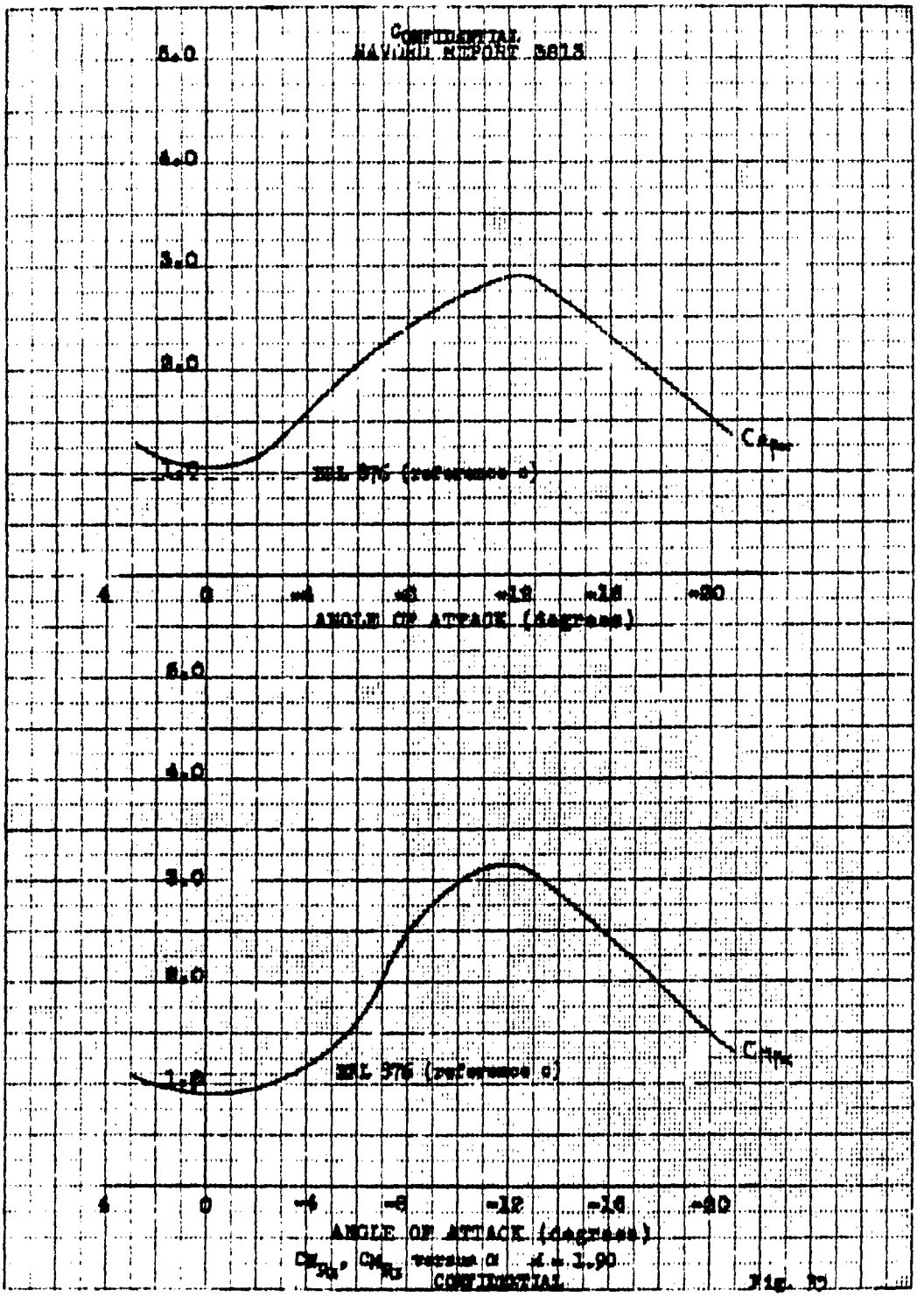

$C_{m_{q_w}}$, $C_{m_{q_c}}$ versus α for $M = 1.90$

CONFIDENTIAL

Fig. 35

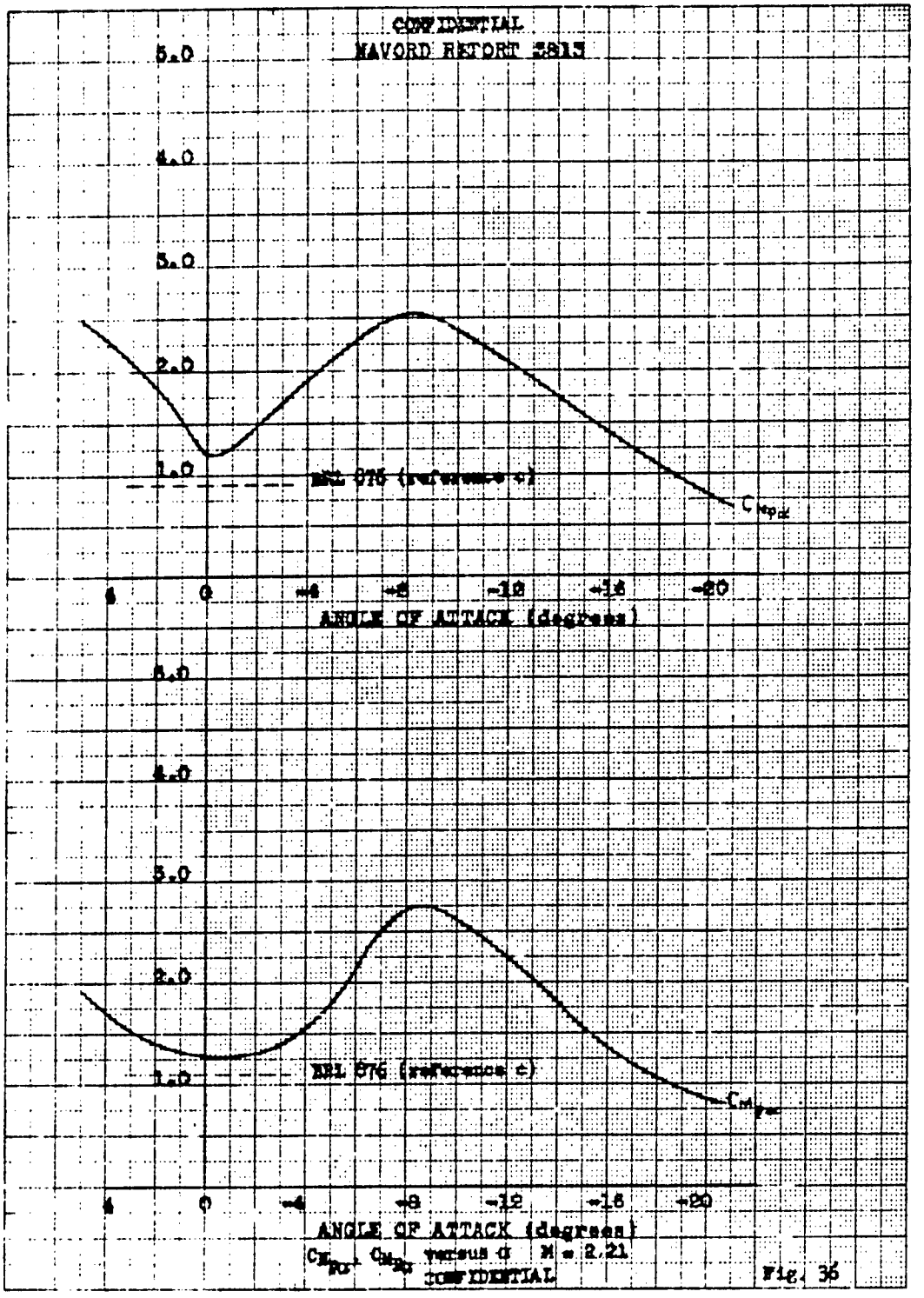

$C_{N_{pc}}$, $C_{m_{pc}}$ versus α M = 2.21

CONFIDENTIAL

Fig. 36

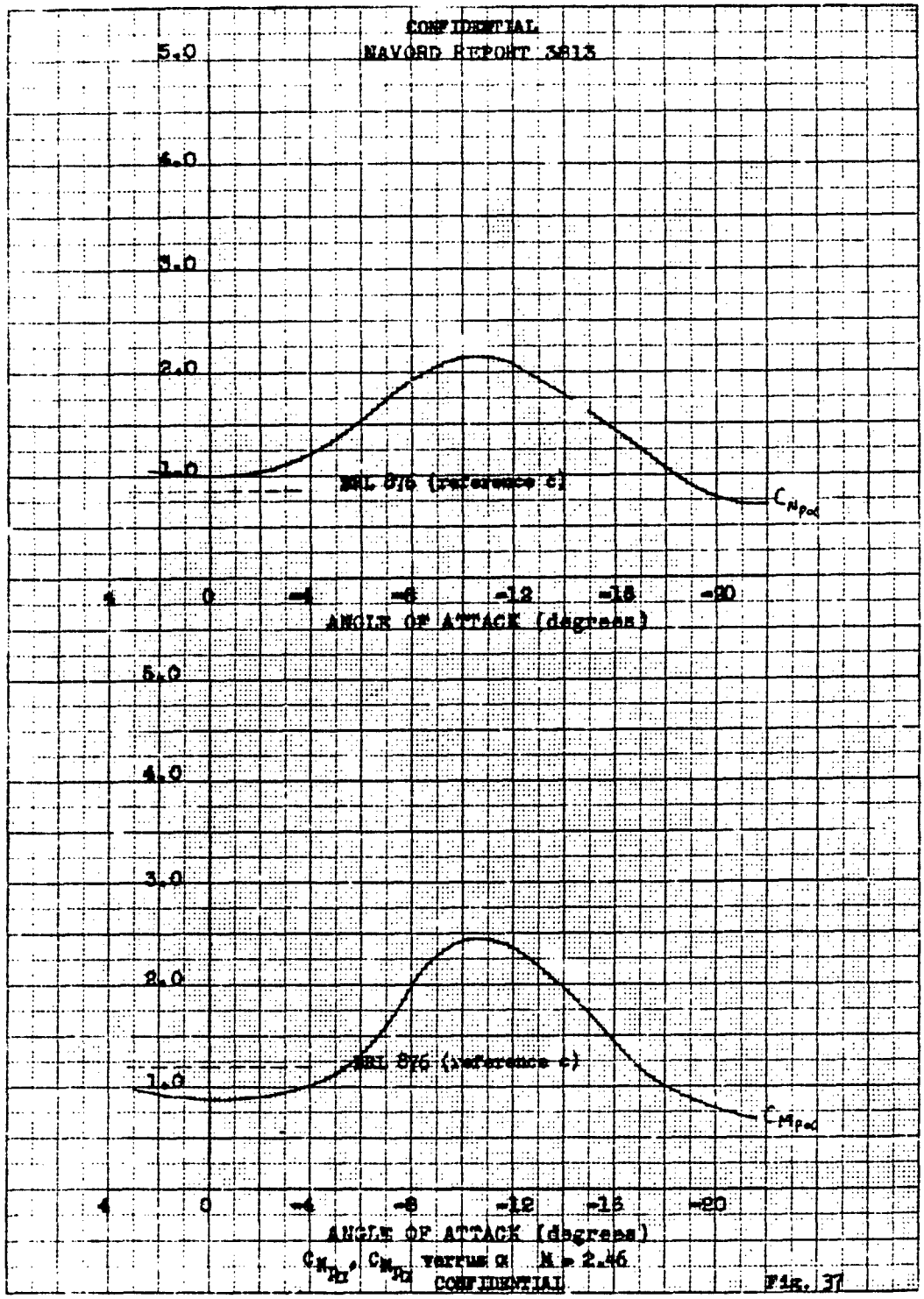

$C_{N_{P\alpha}}$, $C_{M_{P\alpha}}$ versus α M = 2.46

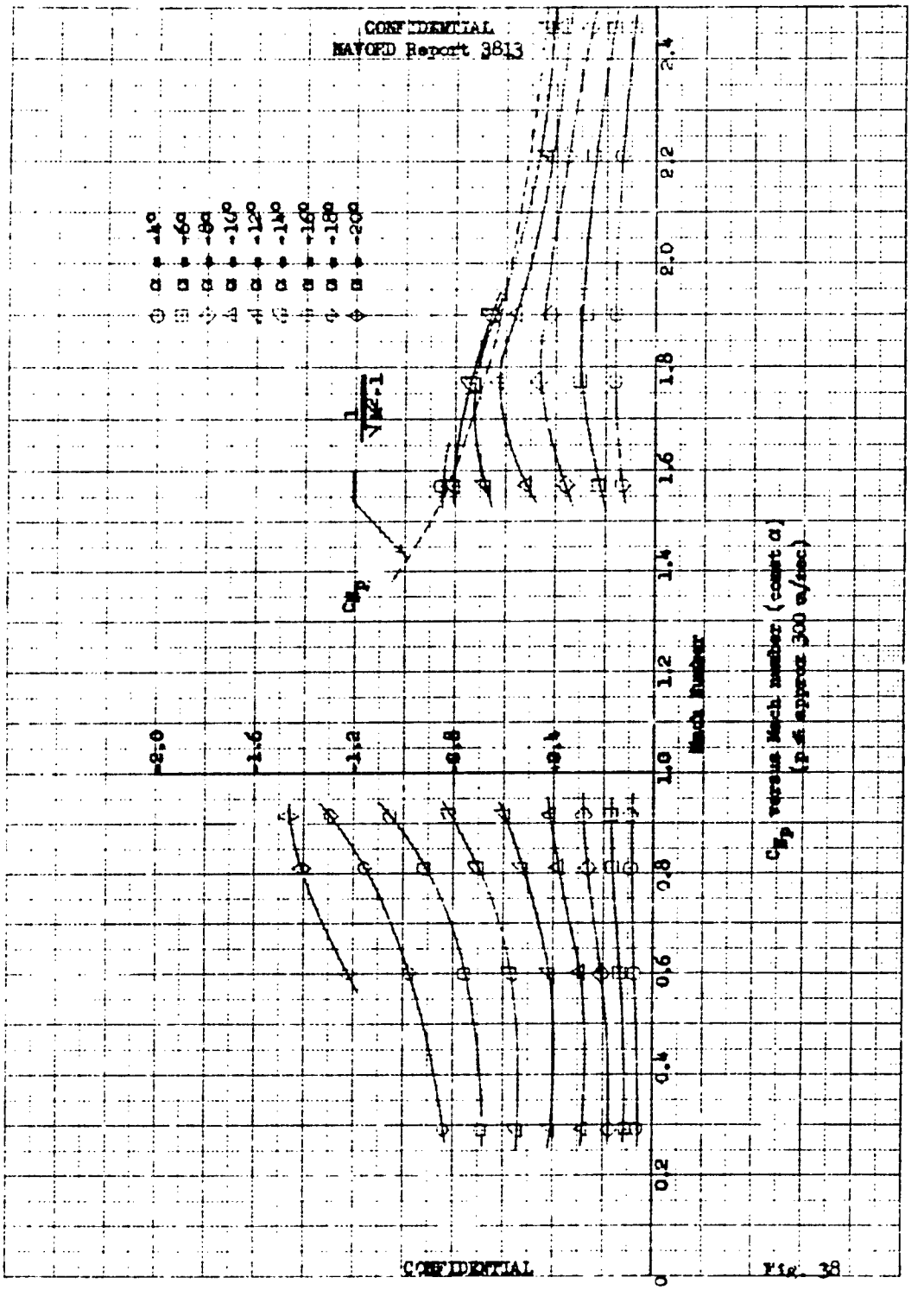
-4°
-6°
-8°
-10°
-12°
-14°
-16°
-18°
-20°
$\frac{1}{\sqrt{M^2-1}}$
C_{N_p}
-2.0
-1.6
-1.2
-0.8
-0.4
0
0.2
0.4
0.6
0.8
1.0
1.2
1.4
1.6
1.8
2.0
2.2
2.4
Mach number
C_{N_p} versus Mach number (const α)
(p& approx 300 #/sec)

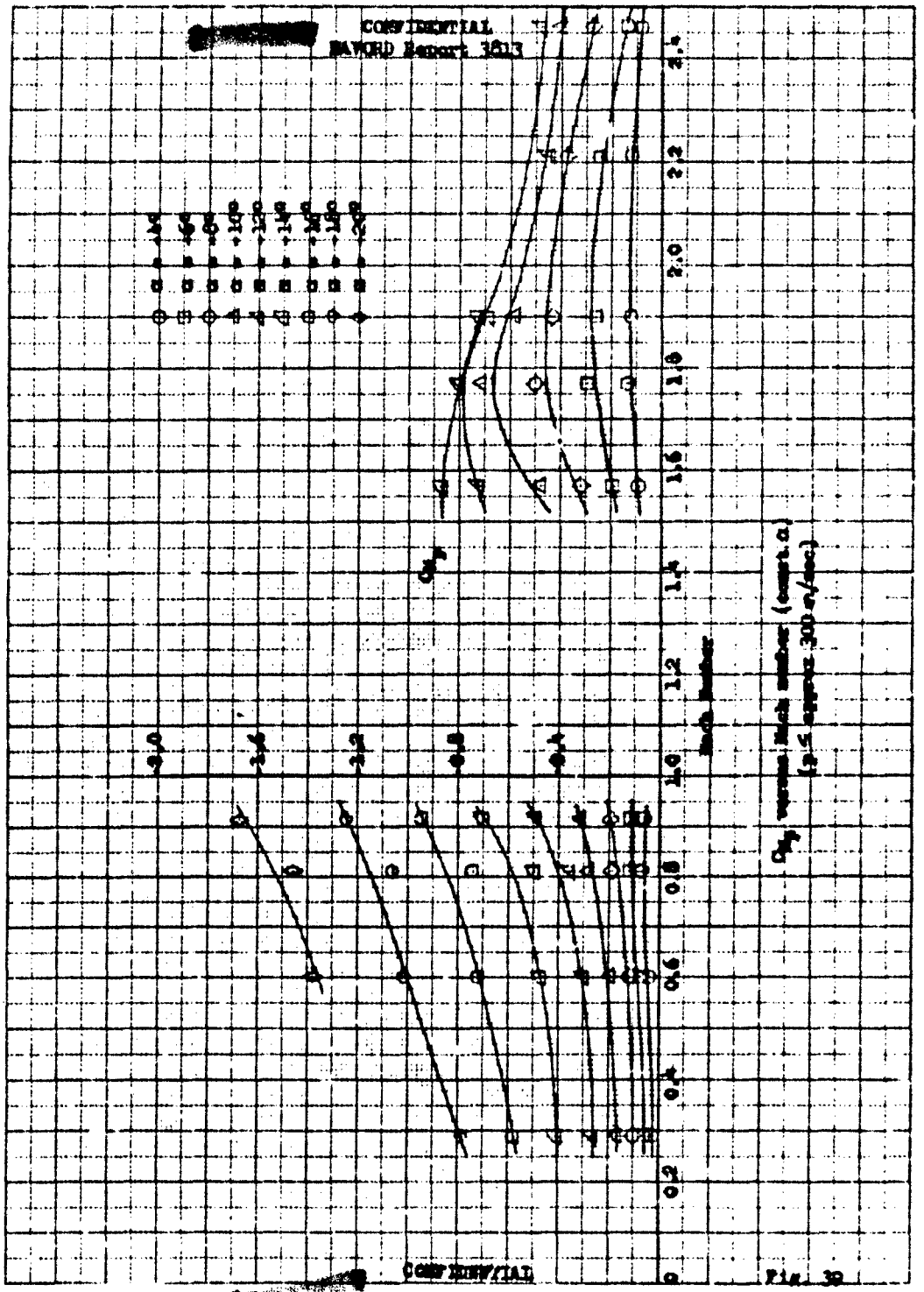

Fig. 30

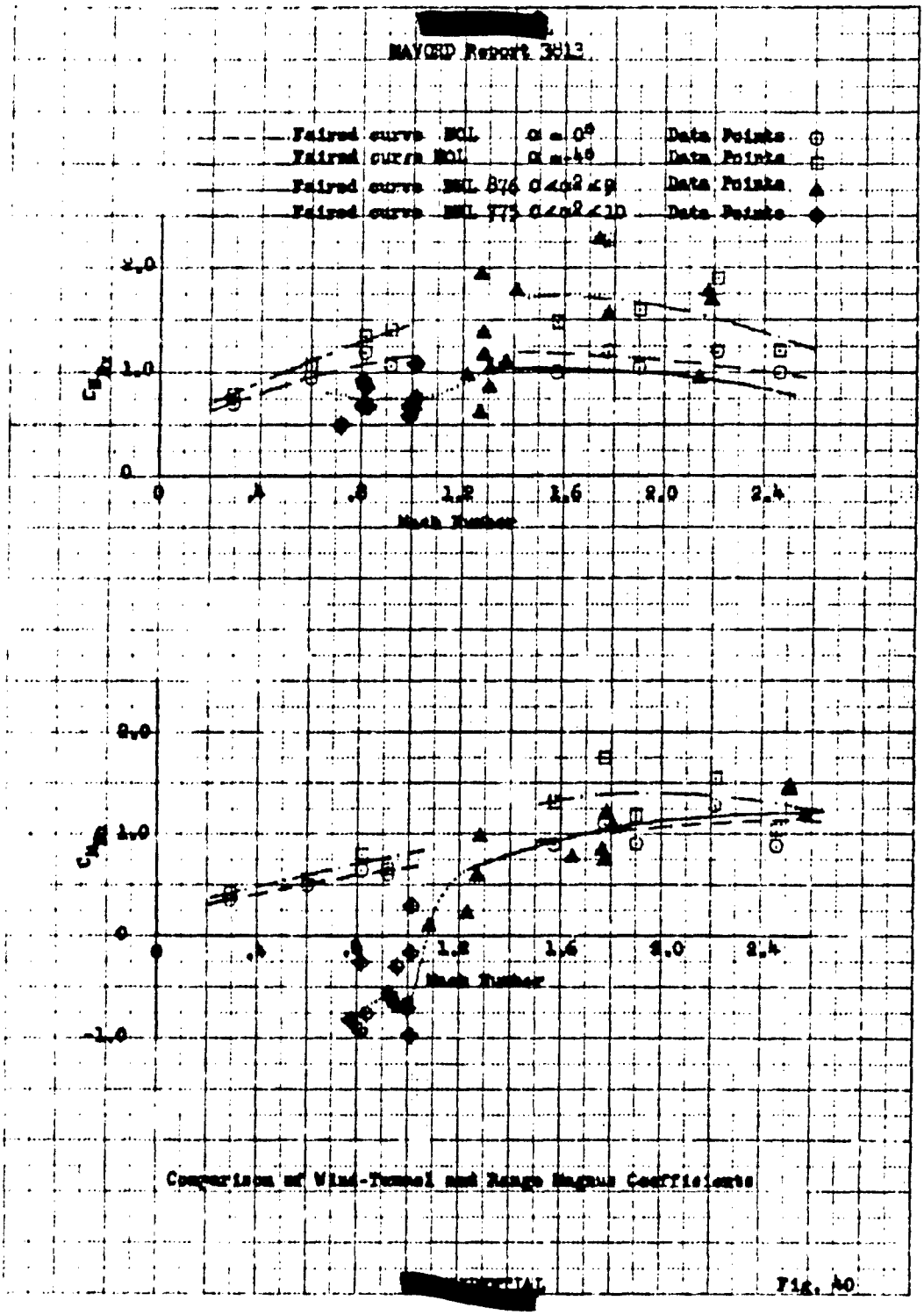

Comparison of Wind-Tunnel and Range Magnus Coefficients

[redacted]

Fig. 40

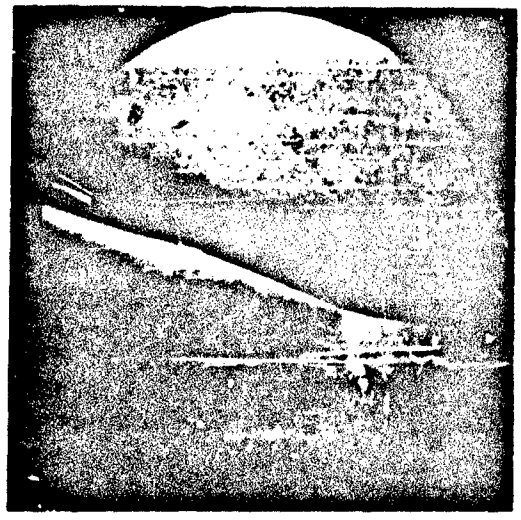

M=0.810 α=21° P=500 N/SEC

M=0.914 α=21° P=500 N/SEC

FIG. 41 TYPICAL SCHLIEREN PHOTOGRAPHS

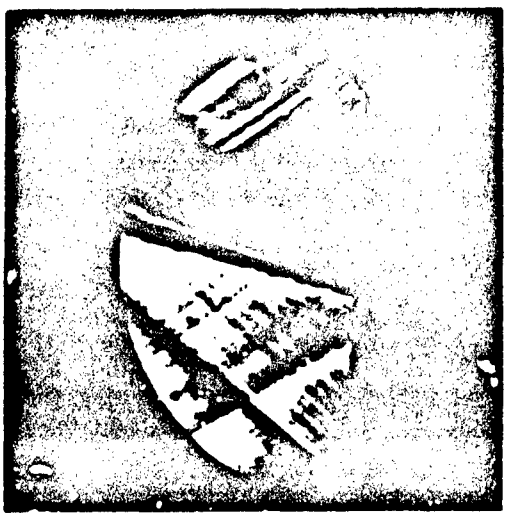

M=1.57 α = -21° P=600 N/SEC

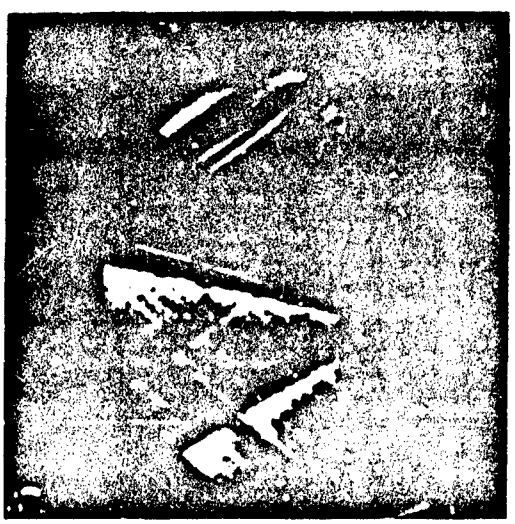

M = 1.57 α = 21° P = 1

FIG. 42 TYPICAL SCHLIEREN PHOTOGRAPHS

[redacted]

EXTERNAL DISTRIBUTION LIST

	No. Copies
Chief, Bureau of Ordnance Department of the Navy Washington 25, D. C.	
Attn: Re3d	2
Re9a	1
Commander U. S. Naval Ordnance Test Station Inyokern, California	
Attn: Dr. I. E. Highberg	2
H. R. Kelley	1
Director National Advisory Committee for Aeronautics Langley Air Force Base, Virginia	1
Attn: J. Bird	1
Washington Office National Advisory Committee for Aeronautics 1724 F Street, N. W. Washington 25, D. C.	1
Ames Aeronautical Laboratory Moffett Field, California	
Attn: Dr. A. C. Charters	1
V. A. Allen	1
Ballistics Research Laboratories Building 45 Aberdeen Proving Ground, Maryland	
Attn: C. H. Murphy	1
C. L. Poor	1
B. Karpov	1
Consolidated Vultee Aircraft Corporation Daingerfield, Texas	
Attn: R. J. Volluz	2
Naval Supersonic Laboratory Massachusetts Institute of Technology Cambridge, Massachusetts	
Attn: L. Schindel	1
Jet Propulsion Laboratory California Institute of Technology 4800 Oak Grove Drive Pasadena, California	
Attn: F. Goddard	1

[redacted]

EXTERNAL DISTRIBUTION LIST (continued)

	No. Copies
United Aircraft Corporation East Hartford 8, Connecticut Attn: I. Twomey	1
David Taylor Model Basin Carderock, Maryland Attn: R. T. Patterson	1
Commanding General WADC Wright Patterson Air Force Base, Ohio Attn: Armament Branch	1
Consolidated Vultee Aircraft Corporation San Diego, California Attn: Dr. G. L. Shue	1
Cornell Aeronautical Laboratory Buffalo, New York Attn: A. H. Flax	1
Redstone Arsenal Huntsville, Alabama Attn: E. B. May	1
Commander U. S. Naval Air Missile Test Center Point Mugu, California Attn: C. Aldridge Wind-Tunnel Section	1 1
Midwest Research Institute 4040 Pennsylvania Kansas City 2, Missouri	1